



University of
Stavanger

Faculty of Science and Technology

MASTER'S THESIS

Study program/Specialization: Petroleum Geosciences Engineering	Spring, 2017 Open
Writer: Per Kristian Malde	<hr/> (Writer's signature)
Faculty supervisor: Nestor Cardozo External supervisors: Jan Tveiten, Schlumberger Per Salomonsen, Schlumberger	
Title of thesis: Coupling of trishear fault-propagation folding and ground process modelling.	
Credits (ECTS): 30	
Keywords: Trishear GPM Extensional fault-propagation folding Forward modelling Growth-strata Eustatic sea level curve Relay ramp	Pages: 87 +enclosure: 11 Stavanger, June 15th , 2017

Copyright
by
Per Kristian Malde
2017

**Coupling of trishear fault-propagation folding and ground process
modelling.**

by

Per Kristian Malde

Master's Thesis

Presented to the Faculty of Science and Technology

The University of Stavanger

The University of Stavanger

June, 2017

Acknowledgements

I would like to express my gratitude to my supervisor Nestor Cardozo for his guidance, knowledge, patience, and encouragement through this thesis. I appreciate all the help he has provided in form of Matlab scripts, discussions, valuable comments, and much more.

I would like to thank my external supervisors Jan Tveiten and Per Salomonsen, for their expertise in successfully linking the Matlab scripts with GPM and Petrel. I appreciate all the help, numerous technical support emails, and simulating tips provided.

Many thanks also to Andreas Habel in IT support. Additionally, I would like to thank my classmates for a positive and thriving class environment through my Master studies.

This thesis is dedicated to the memory of my beloved father, Kristian Malde, September 5th, 2016.

Abstract

Coupling of trishear fault-propagation folding and ground process modelling.

Per Kristian Malde, Master of Science (MSc)

The University of Stavanger, 2017

Supervisors: Nestor Cardozo

External Supervisors: Jan Tveiten and Per Salomonsen

This thesis couples two processes, tectonics and sedimentation, by simulating the kinematics of fault-propagation folding with sedimentary processes in the form of erosion, transport, and deposition, in a 3D numerical forward tectono-sedimentary model. This model couples two programs: trishear (Erslev, 1991; Cardozo, 2008) as Matlab scripts for the kinematic simulation of fault propagation folding, and GPM a Petrel plugin for ground process modelling (Tetzlaff et al., 2014). A link between these two programs was established, to send results and communicate during the simulation. The dynamic relationship between tectonics and sedimentary processes is well illustrated in the models presented, which are divided in two cases: i. A single normal fault propagating with various trishear parameters along strike, or with constant trishear parameters and various GPM parameters. ii. An extensional relay ramp, first, with an overall slope controlled diffusion process, then with an unsteady flow process simulating turbidites. Trishear kinematics combined with GPM simulates a forward physical depositional environment where the sedimentary processes accommodate the tectonic response in a realistic manner. Thus, growth-strata geometries combined with tectonic deformation are significantly influenced by tectonic uplift and sea level changes, resulting in distinct system tracts. Since the model is embedded in Petrel, visualisation of the resultant depositional geometries, either as cross sections or Wheeler diagrams, is straightforward. The potential for further developing this implementation is significant, either by further elaborating the tectonic or sedimentary models (e.g. compressional folds, salt tectonics, carbonates deposition), or by post-processing the model results for fluid flow or seismic response.

Table of Contents

List of Tables	viii
List of Figures	ix
1 INTRODUCTION	1
2 METHODOLOGY	5
2.1 Trishear modelling	5
2.2 Geologic process modelling (GPM)	6
2.3 Coupling GPM and trishear	9
3 RESULTS	12
3.1 First set of models: Single normal fault simulations	12
3.1.1 K model – Constant trishear parameters	14
3.1.2 VFS model – Variation of fault slip along strike	18
3.1.3 VTA model – Varying trishear angle along strike	25
3.1.4 VPS model – Varying P/S along strike	30
3.1.5 SLD Model – Sea level drop.....	34
3.1.6 Sinrise model – Sinusoidal rise of sea level.....	38
3.2 Relay ramp	44
3.2.2 Relay ramp with diffusion	47
3.2.3 Relay ramp with unsteady flow	51
4 DISCUSSION	55
5 CONCLUSIONS	58
6 REFERENCES	59

List of Tables

TABLE 1: ENVIRONMENTAL VARIABLES THAT ARE USED WHEN CALLING TRISHEAR FROM GPM.	9
TABLE 2: FILES NEEDED TO COUPLE SEDIMENTATION (GPM) AND TRISHEAR (MATLAB). NOTICE THAT THE TRISHEAR SCRIPTS ARE INCLUDED IN THE APPENDIX.	10
TABLE 3: DIFFERENT SIMULATIONS AND THEIR CORRESPONDING PARAMETERS. THE LIGHT GREY CELLS REPRESENT THE PARAMETERS FOR TRISHEAR, AND THE DARK GREY CELLS ARE THE PARAMETERS FOR GPM.....	14

List of Figures

FIGURE 1: SCHEMATIC ILLUSTRATION OF AN EXTENSIONAL FAULT-PROPAGATION FOLD WITH A RAMP DIPPING AT AN ANGLE OF 60 DEGREES, ILLUSTRATING THE PARAMETERS OF THE TRISHEAR MODEL.....	2
FIGURE 2: SCHEMATIC ILLUSTRATION WHERE THE DASHED LINE SHOWS INITIAL TOPOGRAPHY AND THE BLACK LINE SHOWS THE NEW TOPOGRAPHY, AFTER DIFFUSION. DASHED AREA REPRESENTS EROSION, AND RED AND BLUE AREA SHOWS DEPOSITION. SEDIMENTS DEPOSITED HAVE DIFFERENT TRANSPORTABILITY, COARSE (RED) AND FINE (BLUE) (GPM USER TUTORIAL, 2016).	7
FIGURE 3: COUPLING OF GPM AND TRISHEAR (MATLAB) AS A SIMPLE FLOWCHART.	11
FIGURE 4: THE FOUR COLOUR COMPONENTS USED TO DISPLAY GRAIN SIZE IN THE MODELS (MODIFIED FROM GPM USER TUTORIAL, 2016).....	13
FIGURE 5: TECTONO-SEDIMENTARY MODEL WITH A 60° DIPPING NORMAL FAULT WITH A SLIP RATE OF 1 M/KA. THE TRISHEAR ANGLE IS 60°, AND THE P/S IS 2. TOTAL RUN-TIME IS 100 KA, AND THE VERTICAL EXAGGERATION IS 3. THE TRANSPARENT BLUE SURFACE AT ZERO ELEVATION IS THE SEA LEVEL. THE ORANGE TRANSPARENT PLANE REPRESENTS THE FAULT PLANE. THE GPM PARAMETERS USED FOR THIS MODEL ARE DIFFUSION RATE OF 0.07 M²/A AND A SINUSOIDAL SEA LEVEL CURVE WITH AN AMPLITUDE OF 50 M. AXES ARE IN METERS.	13
FIGURE 7: A) SCHEMATIC ILLUSTRATION OF A NORMAL FAULT ASSOCIATED WITH LATERAL AND VERTICAL PROPAGATION OF FAULT TIP. THE BLOCK DIAGRAM ILLUSTRATES THE BEHAVIOUR OF MONOCLINAL FOLDS ALONG STRIKE (MODIFIED FROM GAWTHORPE ET AL., 1997). THE RED DASHED RECTANGLE INDICATES THE LOCATION OF B AND MODEL VFS. B) SCHEMATIC ILLUSTRATION DISPLAYING THE CONCEPT OF VARYING FAULT SLIP RATE AND THE EXTENT OF THE MODEL VFS (RED DASHED SQUARE). THE PURPLE AREA SHOWS WHERE THE REST OF THE SEDIMENTARY WEDGE AND THE FAULT TIPLINE WOULD BE.....	18
FIGURE 8: CROSS SECTIONS SHOWING THE EFFECT OF VARIOUS SLIP RATES AT OPPOSITE FAULT TIPS. A) WESTERN FAULT TIP WITH SLIP RATE = 0.5 M/KA. B) EASTERN FAULT TIP WITH SLIP RATE = 1 M/KA. IN BOTH CASES, (I) AND (II) ARE THE INITIAL AND FINAL STAGE, RESPECTIVELY. DASHED LINE IN THE FINAL STAGE OF B INDICATES THE HANGING WALL ELEVATION. THE MODEL HAS P/S = 2 AND TRISHEAR ANGLE = 60°.	20

FIGURE 9: ALONG STRIKE CROSS SECTION AND WHEELER DIAGRAM OF VFS MODEL AT 100 KA. A) MAP VIEW SHOWING THE LOCATION OF THE CROSS SECTION AND WHEELER DIAGRAM (Y = 600). B) CROSS SECTIONS DISPLAYING THE EASTERN TILTING OF THE MODEL, LEADING TO SEDIMENTS DEPOSITING AS A WEDGE. C) WHEELER DIGRAM SHOWING THE CONDENSATION OF COARSE SEDIMENTS (GREEN AND RED) IN THE WEST COMPARED TO THE EAST.	21
FIGURE 11: CROSS SECTIONS SHOWING THE IMPACT OF DIFFERENT TRISHEAR ANGLES AT OPPOSITE FAULT TIPS. A) WESTERN FAULT TIP WITH A TRISHEAR ANGLE OF 100°. B) EASTERN FAULT TIP WITH TRISHEAR ANGLE OF 40°. IN BOTH CASES (I) IS THE INITIAL STAGE, AND (II) IS THE FINAL STAGE. THE MODEL HAS FAULT SLIP RATE = 1 M/KA, AND P/S = 2.....	25
FIGURE 13: SCHEMATIC ILLUSTRATION DISPLAYING DIFFERENT P/S RATIOS ON PROPAGATING NORMAL FAULT, WITH A RAMP OF 60° AND TRISHEAR ANGLE = 60°. A) P/S = 1, TIGHTER MONOCLINE WITH STEEP FORELIMB. B) P/S RATIO = 4, BROADER MONOCLINE AND FAULT BREACHING THE FOLD.	30
FIGURE 18: SCHEMATIC ILLUSTRATION DISPLAYING A RELAY RAMP STRUCTURE AT AN EARLY STAGE, WITH RELATED TERMS. (MODIFIED AFTER ATHMER AND LUTHI, 2010)	45
FIGURE 19: SKETCH OF THE GRID WITH THE LOCATION OF THE FAULTS, AND THE WIDTH BETWEEN THE FAULTS. THE GRID IS 2000 M X 2000 M AND CONTAINS 10 000 CELLS. BLACK ARROWS SHOW THE MAGNITUDE AND SENSE OF FAULT MOVEMENT. THE FAULTS HAVE CONSTANT SLIP RATE ON THE SIDES, AND THE SLIP RATE DECREASES TO ZERO TOWARDS THE MIDDLE OF THE MODEL. NOTE THAT THE FAULTS DIP NORTH.	45
FIGURE 20: ELEVATION OF RELAY RAMP MODEL OVER TIME. A) MODEL'S INITIAL STATE. B) 20, C) 40, D) 60, E) 80 AND F) 100 KA. ONLY TECTONIC DEFORMATION IS SHOWN.....	46
FIGURE 21: EVOLUTION OF RELAY RAMP MODEL WITH DIFFUSION AS MAP VIEWS OVER TIME. THE BLACK DASHED LINE IS THE COASTLINE. A) 0, B) 20, C) 40, D) 60, E) 80 AND F) 100 KA.	48
FIGURE 22: RELAY RAMP MODEL WITH DIFFUSION, WITH CORRESPONDING E-W CROSS SECTIONS AND WHEELER DIAGRAMS (1 AND 2). THE MODEL IS DISPLAYED AT THE FINAL STAGE 100 KA, THE COLORS REPRESENT DIFFERENT FACIES. CROSS SECTIONS HAVE 3X VERTICAL EXAGGERATION.	49

- FIGURE 23: N-S CROSS SECTIONS AND WHEELER DIAGRAMS OF THE RELAY RAMP MODEL IMPLEMENTED WITH DIFFUSION. LOCATION OF THE SECTIONS IS ON THE MAP VIEW IN THE PREVIOUS FIGURE. THE MODEL IS DISPLAYED AT THE FINAL STAGE 100 KA, AND THE COLOURS REPRESENT DIFFERENT FACIES. THE CROSS SECTIONS HAVE 3X VERTICAL EXAGGERATION.50**
- FIGURE 24: RELAY RAMP MODEL AS ELEVATION MAPS, WHERE WARM COLOURS REPRESENT HIGH ELEVATION AND COLD COLOURS REPRESENT LOW ELEVATION. A) MODEL'S INITIAL STATE WITH THE OUTLINE OF THE SOURCE, B) 20, C) 40, D) 60, E) 80 AND F) 100 KA, INCLUDING FAULTS MARKING THE RELAY RAMP AND ARROWS REPRESENTING INCISED CHANNELS AND DIRECTION OF FLOW.....52**
- FIGURE 25: MAP VIEW OF THE RELAY RAMP MODEL WITH THE UNSTEADY FLOW AT 100 KA. BLACK DASHED LINE IS THE INTERPRETATION OF THE DEPOSITIONAL MORPHOLOGY. FLOW IS ILLUSTRATED WITH BLUE COLOURS FROM SW TOWARDS NE. FACIES ARE SHOWN IN THE OUTER RIM OF THE MAP. BLACK LINES ARE THE SECTIONS IN FIGURE 26.....53**
- FIGURE 26: CROSS-SECTIONS THROUGH THE RELAY RAMP MODEL WITH THE UNSTEADY FLOW AT 100 KA. SECTIONS 1 - 3 STRIKE E-W, AND 4 - 6 N-S. AXES ARE IN METERS. RED LINES WITHIN SEDIMENTARY PACKAGES REPRESENT CYCLES OF 2 KA. LOCATION OF SECTIONS CORRESPONDS WITH THE MAP IN THE PREVIOUS FIGURE. RECTANGLES ON SECTIONS SHOW ZOOMED AREAS. NO VERTICAL EXAGGERATION.54**

1 INTRODUCTION

Tectonics and sedimentation are two significant geological processes that often occur simultaneously and affect each other. Tectonics provide a first-order control on sedimentation by influencing topography (e.g. slope gradient) and the sediment source area. Tectonics affects denudation rates, accommodation space, thickness, size and location of the sediments, and acts as a major control on sea level. Sea level influences sedimentary processes and environments, controlling sediment properties and stratigraphy.

Some depositional basins form as result of tectonic processes such as faulting. Faults occur in various styles and can be classified based on their direction of slip (i.e. dip, strike or oblique-slip). This thesis examines normal faults and folds formed by the propagation of these faults, i.e. extensional fault-propagation folds. Hydrocarbon accumulations are often present in these structures or in the underlying fault blocks (Gawthorpe and Hardy, 2002).

The objective of this thesis is to couple the kinematic process of fault-propagation folding with erosion, transport, and deposition through numerical tectono-sedimentary modelling in three-dimensions (3D). This is accomplished by integrating the trishear kinematic model (Erslev, 1991; Allmendinger, 1998; Hardy and Allmendinger, 2011), with the ground process modelling software GPM (Schlumberger). GPM is an experimental stratigraphic forward modelling software, where tectonics can be modelled as vertical movement of the basement (base level; Tetzlaff *et al.*, 2014).

Trishear is a kinematic model for fault-propagation folding (Figure 1) that consumes the decrease in displacement along the fault using heterogeneous shear in a triangular zone radiating from the tip line (Erslev, 1991; Allmendinger, 1998). The parameters for trishear are the coordinates of the fault tip, the ramp angle or fault dip angle, the fault propagation to slip ratio (P/S), the apical angle of the triangular zone or trishear angle, and the fault slip. In 3D, these parameters can vary along strike (Cardozo, 2008). Fault-propagation folds and trishear-like deformation play an important role in extensional fault systems, controlling fault propagation, fault linkage, and sedimentation (Gawthorpe and Hardy, 2002).

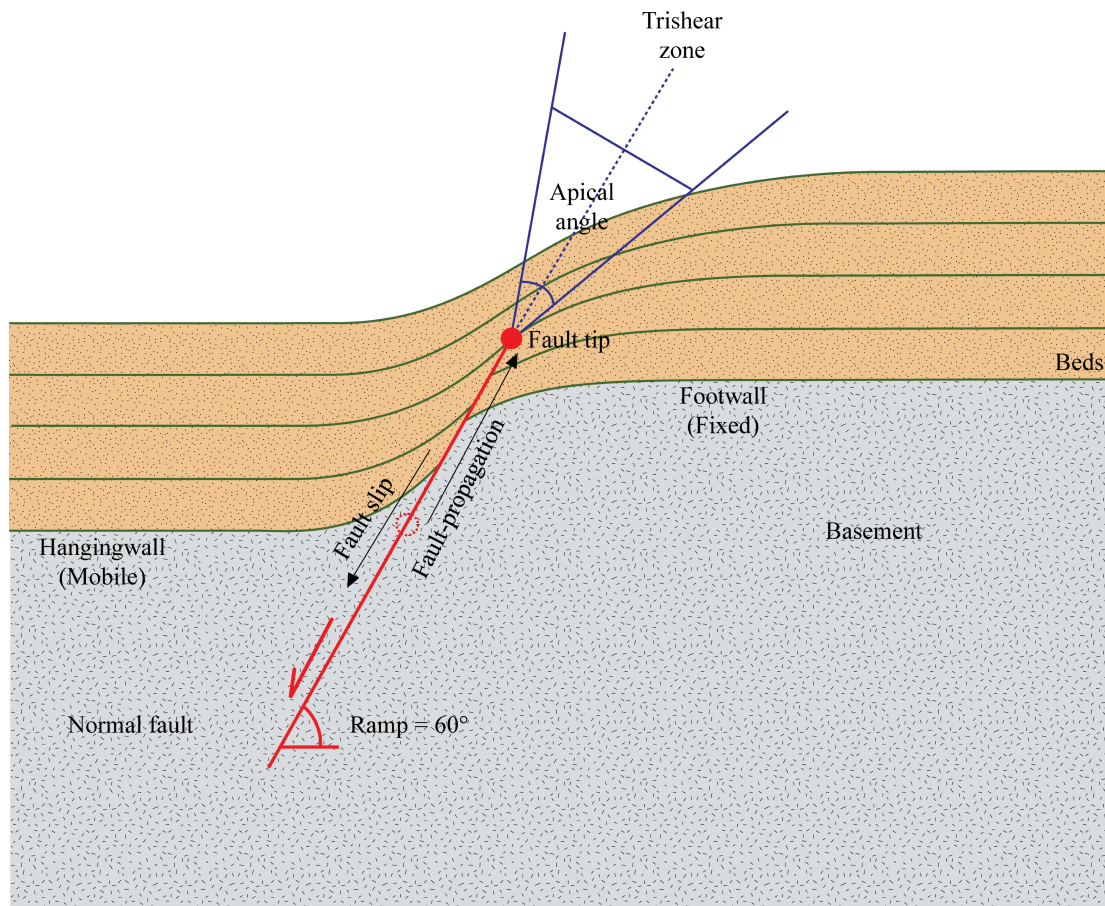


Figure 1: Schematic illustration of an extensional fault-propagation fold with a ramp dipping at an angle of 60 degrees, illustrating the parameters of the trishear model.

Outcrop and analogue modelling studies in extensional settings show that a monocline usually occurs above blind normal faults, and as displacement increases, the fault propagates upwards breaching the fold (Hardy and Ford, 1997). The growth strata geometries are strongly influenced by the fault-propagation to slip ratio (P/S) and the width of the deformation zone (trishear angle, Figure 1). Gawthorpe and Hardy (2002) used a kinematic model of fault-propagation folding coupled with a sedimentary model for coarse-grained deltaic clastic sediments, to investigate these growth strata geometries. Their case study uses a two-dimensional model and highlights the importance of integrating structural and stratigraphic processes, which address fault-propagation folding kinematics and sedimentation.

This project addresses mainly two cases. The first case models one propagating normal fault, and the second case explores two propagating normal faults, forming a relay ramp structure. For the first case, I present a series of simulations with varying trishear parameters along strike (i.e. fault slip rate, trishear angle, and P/S) and constant GPM parameters. Then, I present a second set of simulations where trishear parameters are kept constant whereas GPM parameters such as diffusion rate and sea level are varied.

The second case involves two synthetic overlapping (Morley *et al.*, 1990) normal faults with 400 m fault displacement, dying out along strike, and forming a relay structure. In this case, I use fixed trishear parameters under diffusion or point source and unsteady flow in GPM. Unsteady flow is a way to model the input of water and sediments in turbidity currents.

The developed trishear-GPM implementation provides a detail view of the interplay between tectonics and sedimentation in 3D and through time. The results show the influence of fault kinematics and controlling trishear parameters on depositional architecture and growth strata geometries. They also demonstrate the influence of eustatic sea level on the 3D geometry and evolution of growth strata. This study highlights the importance of integrating structural and sedimentary processes into a forward tectono-sedimentary model that produces a realistic and rich stratigraphy. Using the model, it is possible to reconstruct conditions comparable to those encountered in nature. For exploration purposes, the model can work as a decomposition tool to better target and understand sedimentary reservoirs. It can also improve stratigraphic correlations from well logs and seismic data.

2 METHODOLOGY

2.1 Trishear modelling

Eric Erslev published the trishear model in 1991 (Erslev, 1991). Trishear is a kinematic model for fault-propagation folding that preserves the decrease in displacement along the fault using heterogeneous shear in a triangular zone radiating from the tip line (Erslev, 1991; Allmendinger, 1998). The parameters in the trishear model are the location of the fault tip, fault dip, fault propagation to slip ratio (P/S), apical angle of the trishear zone or trishear angle, and fault slip (Allmendinger, 1998). When fault dip and fault slip are known, two parameters impact the nature and location of deformation: the trishear angle and the P/S. The trishear angle or apical angle of the trishear zone affects the width of the deformation above the fault tip, whereas the P/S ratio affects how fast the fault propagates through the strata (Figure 1; Cardozo, 2008; Hardy and Allmendinger, 2011).

Hardy and Ford (1997) expanded the original trishear model further for application to more general scenarios. In their model, the trishear zone is attached to the fault tip and propagates upward through the overlying material (Figure 1). Allmendinger (1998) implemented Hardy and Ford (1997) model and showed that trishear sufficiently explains the geometry, strain, and fracture orientations of fault-propagation folds in the field and analog experiments. These two studies look at trishear in two-dimensions (2D).

A pseudo-3D model is a reasonable strategy for modelling trishear in 3D as shown by Cardozo (2008). The pseudo-3D formulation uses serial cross sections parallel to the slip direction (Cristallini and Allmendinger, 2001) that are all aggregated into a 3D model. This model practically conserves volume during simulations with and without

lateral fault propagation (Cardozo, 2008). It allows changing trishear parameters along strike from one fault tip to the other. This is often done in a linear way, but in fact, any variation of trishear parameters along strike can be implemented in pseudo-3D modelling (Cardozo, 2008). In this thesis, I use a pseudo-3D trishear model with dip slip (slip rake is 90°), linear variation of trishear parameters along strike, and no lateral propagation.

2.2 Geologic process modelling (GPM)

GPM is a sedimentary simulation and visualisation package for stratigraphic forward modelling that is implemented as a Petrel plugin. The software was developed as a research project in 2001-2002 by WesternGeco. From 2003 to 2005, the Schlumberger-Doll Research (SDR) Center improved the software and convert it to an Ocean plugin for Petrel in 2012. Developments are still ongoing at the Schlumberger Research Center (GPM user tutorial, 2016).

GPM models erosion, transport and deposition of clastic sediments as channels, rivers, turbidity systems, and shoreline deposits. Carbonate growth, sediment compaction, fluid expulsion and other processes can also be implemented in this modelling environment. GPM is based on numerical modelling of open-channel flow by modelling a physical system constrained by sedimentary processes (e.g. currents and waves). Other forward modelling packages rely solely on data and spatial statistics, while physical sedimentary processes are not taken into account. This is not the case in GPM, where the simulation is driven by forward physical modelling (Tezlaff et al., 2014).

Initial conditions and boundary conditions (e.g. basin topography, sea level changes, sediment input, flow input from rivers, etc.) need to be specified by the user in order to predict the resultant sedimentary geometries. To start the sedimentation model, an initial Petrel surface or basement must be introduced in the software. This will

establish initial limitations on where erosion, transport, and deposition of sediments will occur. Below the basement, the lithology is assumed homogeneous and infinite (GPM user tutorial, 2016).

The diffusion rate is an important parameter of the program. It is defined as the rate at which sediments are moved downslope proportional to the slope gradient (Tetzlaff *et al.*, 2014). Different sediment types have characteristic transportability. For example, finer sediments are transported more easily than coarse sediments. Diffusion is often combined with other sediment transport methods in order to maintain sub-cell processes in the model. For instance, modelling a river would only move sediments within the river flow and not affect the sediments above water. This is an unrealistic assumption because there are possible slumps, soil creep and biological processes that cause the slope of the bank to change. These processes can occur at a smaller scale and cannot be processed in grid cells. However, they can be modelled together by diffusion (GPM user tutorial, 2016). As sediments move downslope at a rate proportional to the tangent of the slope angle, the topography becomes smoother over time (Figure 2).

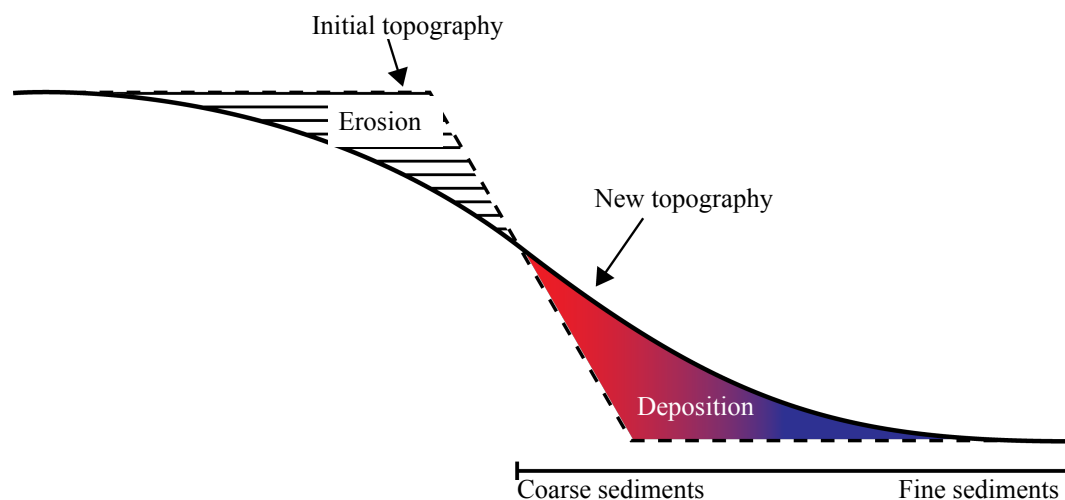


Figure 2: Schematic illustration where the dashed line shows initial topography and the black line shows the new topography, after diffusion. Dashed area represents erosion, and red and blue area shows deposition. Sediments deposited have different transportability, coarse (red) and fine (blue) (GPM user tutorial, 2016).

There are three main controlling factors affecting sea level changes: tectonics leading to uplift or subsidence, eustatic sea level, and sedimentation (Nichols, 2009). In GPM, sea level is initially assumed to be constant at zero elevation, which is the model's datum. There are a variety of methods to model sea level changes (e.g. Haq global sea level, Exxon global sea level, and stratigraphic curve; GPM user tutorial, 2016). The sea level curve is implemented as a sinusoidal or linear function and is visualised in a graph where the x-axis represents age (m.a years), and the y-axis is depth (m) relative to the model's datum.

GPM models input of water and sediments as steady and unsteady flow. Steady flow is better suited for modelling river flows when flow velocity and depth are stable through time. Unsteady flow is a more suitable way to model input of water and sediment in turbidity currents. It uses an algorithm that considers a number of "fluid elements," each representing a small volume of fluid affected by gravity and friction against the surface, and other fluid elements, which simulate the effect of dynamic viscosity (Grigoryev et al., 2002).

Both algorithms estimate erosion, transport action and deposition of sediments, assuming the flow maintains a transport capacity dependent on its velocity and depth. Steady and unsteady flow only allows erosion until the capacity of transport is reached, and will continue transport until the transport capacity decreases to the extent it can no longer carry the load. Different sediment types experience different transportability. Thus steady and unsteady flow handles implicitly the coarser fraction differently than the finer fraction. This simulates the same depositional effect that occurs in nature as a result of different transport types (Tetzlaff *et al.*, 2014). Both algorithms require a source, and a source position map. The user designates the source on a surface with the same dimensions as the initial surface (basement) and provides a source ID distribution. Positive numbers must match the source ID. Negative numbers

are ignored. Henceforth, on the edges an ID of zero indicates a boundary closed to flow, and negative numbers mean a boundary open to flow (GPM user tutorial, 2016).

2.3 Coupling GPM and trishear

In preparation to this workflow, a base “basement” surface must be created in Petrel. After this, the computational procedure starts with setting three environment variables in a command shell (Table 1). These files are the file from GPM (input.csv), the file from trishear (out.csv), and the command to call trishear in Matlab. Notice that this last command runs Matlab in the background.

Table 1: Environmental variables that are used when calling trishear from GPM.

- 1) set GPM_TRI_IN_FILE=input.csv
 - 2) set GPM_TRI_OUT_FILE=out.csv
 - 3) set GPM_TRI_RUN_COMMAND=matlab -nosplash -nodesktop -minimize -wait -r trishear
-

The directory in the command shell needs to match the folder containing the trishear Matlab scripts (see Appendix) and the GPM project (Table 2). The next step is to open Petrel from the command shell by typing its executable path, ("C:\Program Files\Schlumberger\Petrel 2015\Petrel.exe").

Table 2: Files needed to couple sedimentation (GPM) and trishear (Matlab). Notice that the trishear scripts are included in the Appendix.

	Type	Description/purpose
Matlab	trishear.m	Forward Pseudo-3D trishear (Cardozo, 2008). Reads GPM file, runs trishear, updates fault tips, and write output for GPM.
	veltrishear.m	2D linear velocity field of trishear model (Zender and Allmendinger, 2000). Used to compute trishear deformation in each cross section of pseudo-3D model
	grift.m	Since GPM uses fixed nodes, this script is used to fit the deformed trishear surface at the nodes of the GPM model. gridfit was written by D 'Errico (2006).
Spreadsheet	input.csv	Surface(s) from GPM before trishear deformation. This file is updated by GPM after each timestep.
	out.csv	Surface(s) after trishear deformation. This file is updated by trishear.m after each timestep.
Geo process	gp.exe	The GPM 'engine'.

After these preliminary steps, one should set the parameters for the simulation in a pre-process step (Figure 3). In GPM, the base surface, display steps, and time increments are established by the user. The user should also decide the sedimentary process, e.g. diffusion, compaction, unsteady flow, etc. In Matlab, the user should create a tips.mat file with the initial coordinates of the fault tips. In the script trishear.m (Table 2), the trishear parameters for each fault tip (P/S, trishear angle and fault slip rate), and the timestep should be set by the user. The timestep in trishear.m should be equal to the display step in GPM, and should be such that it produces geologically realistic results, i.e. it couples tectonics and sedimentation realistically, giving the impression that these two processes act simultaneously, although in the computer implementation they happened one after the other.

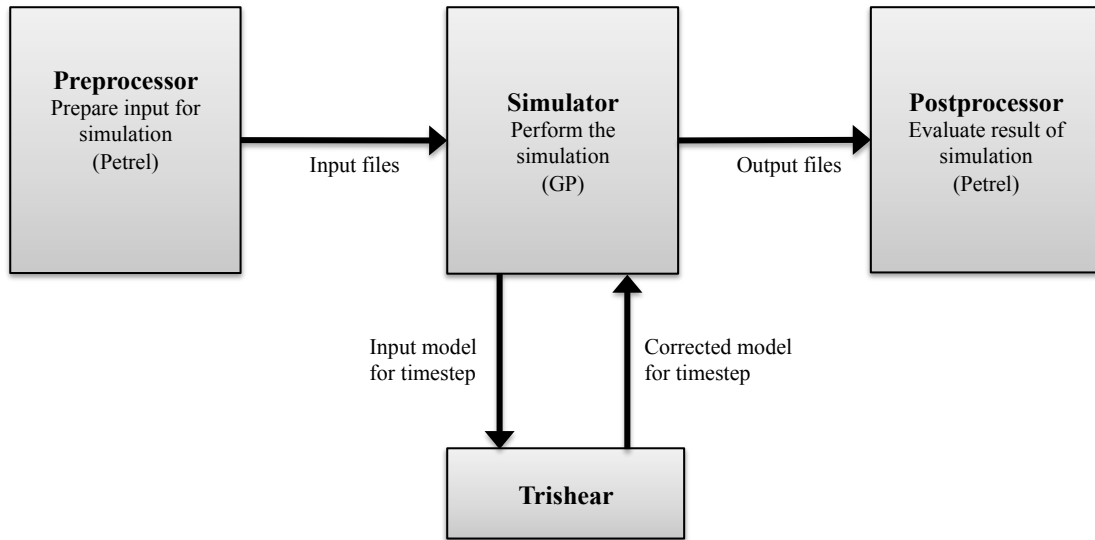


Figure 3: Coupling of GPM and trishear (Matlab) as a simple flowchart.

After this initial setup, the simulation can be executed (Figure 3). At each timestep: (i) GPM runs and write the input file for trishear (gp.exe), (ii) trishear (trishear.m) runs, updates the fault tips (tips.mat), and writes the output file for GPM, and (iii) GPM reads the file from trishear and substitutes its current model. This procedure is repeated for all timesteps.

In each simulation, 50-100 timesteps are run to simulate extensional fault-propagation folding and sedimentation. When the simulation is complete, the post-process step is the final phase (Figure 3). In Petrel, the user can inspect the results of the simulation run as a 3D tectono-sedimentary model.

3 RESULTS

3.1 First set of models: Single normal fault simulations

This section presents examples of the structural, stratigraphic and sedimentary relationships modelled using the methodology discussed in the previous chapter. The colors in the presented models represent four sediment types: coarse sand (red), fine sand (green), silt (blue), and clay (black). The models display variable sediment composition as additive colour mixtures. For example, yellow (Figure 4) represents a mixture of coarse sand with fine sand (Tezlaff et al., 2014). The models in this section involve a 60° dipping normal fault with a total run-time of 100 ka (Figure 5). Each incremental step represents 2 ka, thus there are 50 timesteps in each model. First, a series of simulations are presented with varying trishear parameters along strike and holding GPM parameters constant (Table 3). Then another set of simulations are presented, where trishear parameters are constant, and diffusion rate and sea level are varied in GPM. The models are presented in timesteps of 20 ka between each display, both in map view and cross section. Models with no variation in trishear parameters along strike are shown with a single cross section. Models involving variation of trishear parameters are displayed in two cross-sections, one in the west at $x = 200$ m (B-B'), and another in the east at $x = 800$ m (A-A', Figure 5). Finally, a Wheeler diagram at the end of the simulation is included. The vertical axis of this diagram is time rather than depth (Wheeler, 1964). The Wheeler diagram shows the 50 timesteps from old (bottom) to young (top) where each timestep represents 2 ka. It illustrates facies at a given time and location. A facies running along the diagonal, from bottom left to top right in the Wheeler diagram, implies that sedimentation occurred while the fault was active, similar to growth-strata in seismic.

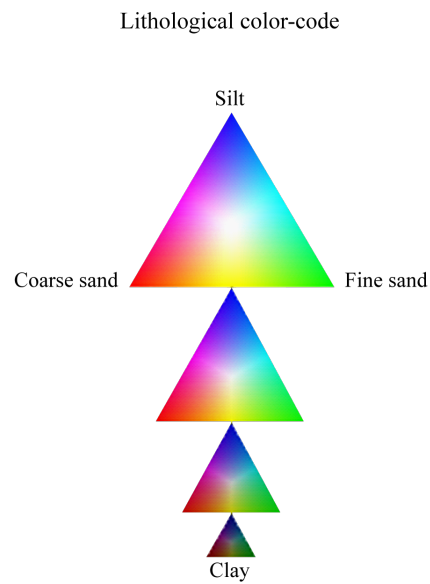


Figure 4: The four colour components used to display grain size in the models (modified from GPM user tutorial, 2016).

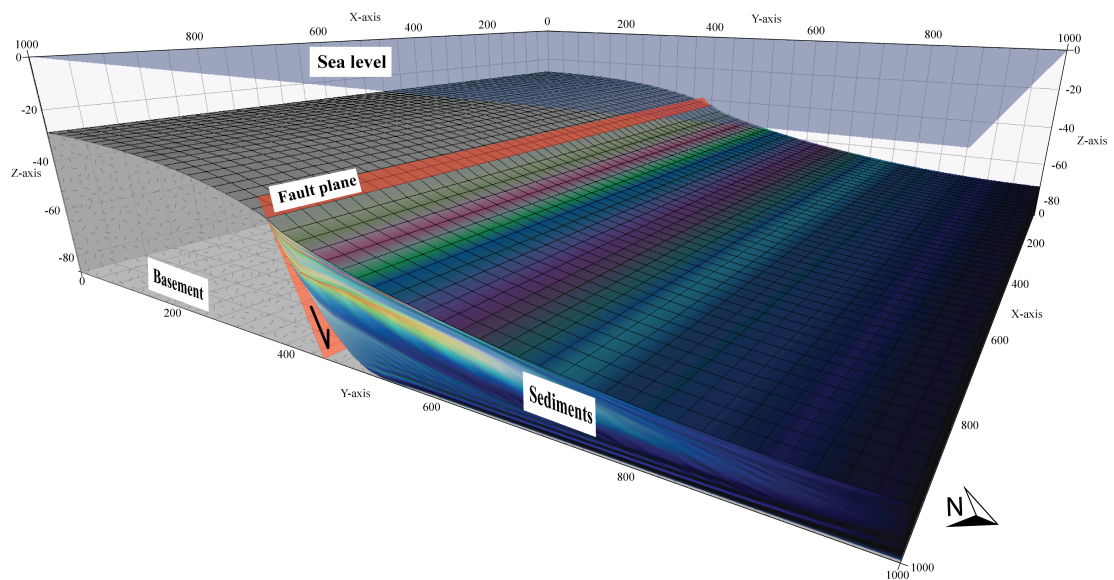
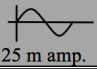
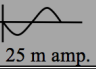


Figure 5: Tectono-sedimentary model with a 60° dipping normal fault with a slip rate of 1 m/ka. The trishear angle is 60° , and the P/S is 2. Total run-time is 100 ka, and the vertical exaggeration is 3. The transparent blue surface at zero elevation is the sea level. The orange transparent plane represents the

fault plane. The GPM parameters used for this model are diffusion rate of $0.07 \text{ m}^2/\text{a}$ and a sinusoidal sea level curve with an amplitude of 50 m. Axes are in meters.

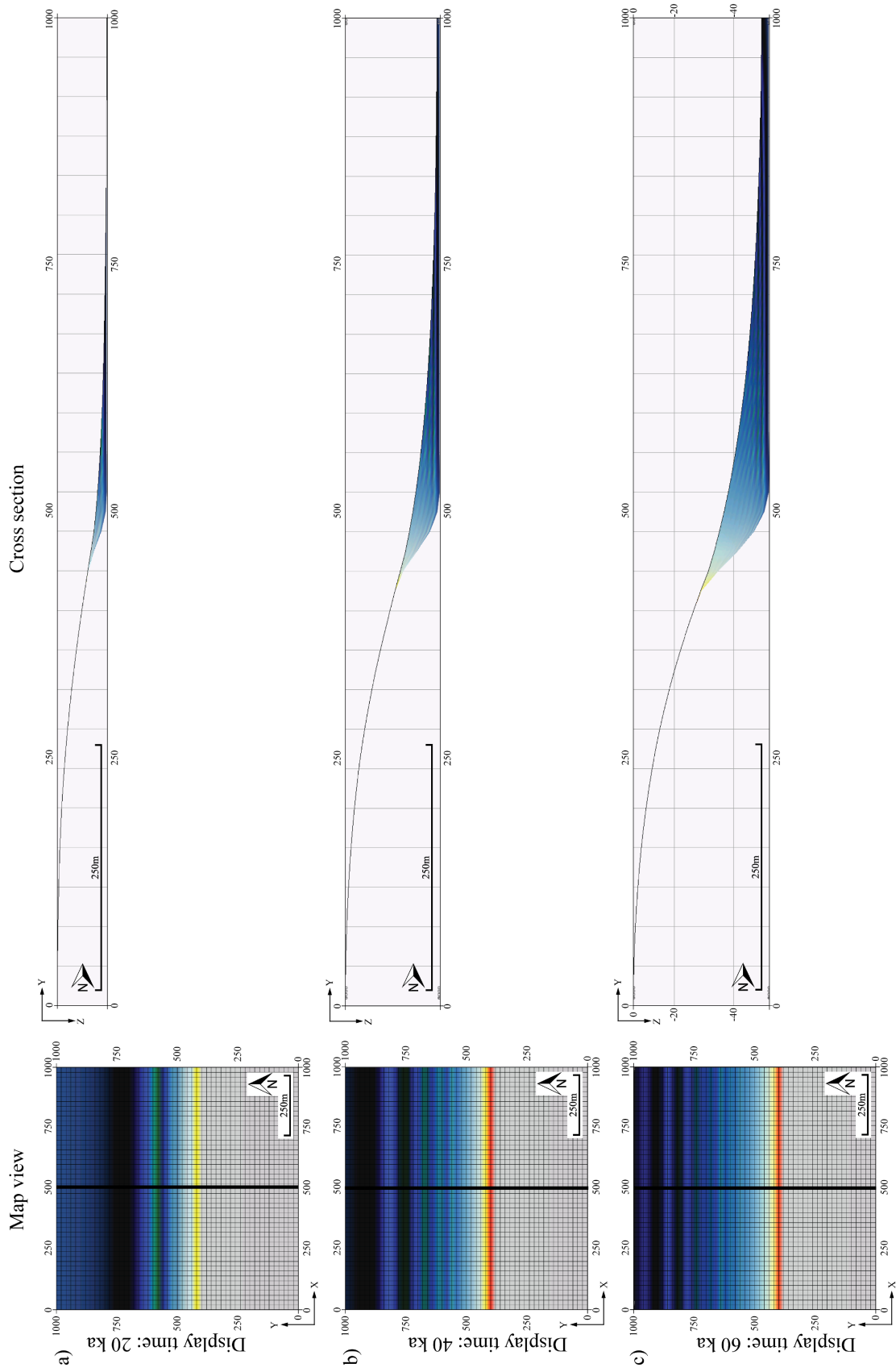
Table 3: Different simulations and their corresponding parameters. The light grey cells represent the parameters for trishear, and the dark grey cells are the parameters for GPM.

	Constant	Variation in fault slip	Variation in trishear angle	Variation in P/S	Diffusion large	Sea level drop	Sea level rise	Sinusoidal rise	Sinusoidal drop
File name:	K	VFS	VTA	VPS	DL	SLD	SLR	SINRISE	SINDROP
Slip rate:	-1 m/ka	Ft1: -1 m/ka Ft2: -0.5 m/ka	-1 m/ka	-1 m/ka	-1 m/ka	-1 m/ka	-1 m/ka	-1 m/ka	-1 m/ka
Trishear angle:	60°	60°	Ft1: 40° Ft2: 100°	60°	60°	60°	60°	60°	60°
P/S:	2	2	2	Ft1: 1 Ft2: 4	2	2	2	2	2
Diffusion rate:	$0.07 \text{ m}^2/\text{a}$	$0.07 \text{ m}^2/\text{a}$	$0.07 \text{ m}^2/\text{a}$	$0.07 \text{ m}^2/\text{a}$	$0.2 \text{ m}^2/\text{a}$	$0.07 \text{ m}^2/\text{a}$	$0.07 \text{ m}^2/\text{a}$	$0.07 \text{ m}^2/\text{a}$	$0.07 \text{ m}^2/\text{a}$
Sea level:	0 m	0 m	0 m	0 m	0 m	-50m Linear	+50m Linear	 25 m amp.	 25 m amp.

3.1.1 K MODEL – CONSTANT TRISHEAR PARAMETERS

First, a basic model is presented with no variation of trishear parameters along strike. Figure 6 shows the sequential progress every 20 ka. The model (K) is run with the parameter values presented in Table 3. During the simulation, the slope steepens developing an upward–widening monocline whose width is controlled by the trishear angle. Sediment accumulation increases proportionally to the slope gradient. The coarse-grained sediments tend to deposit near the slope break, whereas the fine-grained sediments are transported to the more distal regions of the basin (map view, Figure 6). The fault propagates up-section but is not visible until it breaches the overlying fold (Figure 6e). In The Wheeler diagram (Figure 6f), yellow (finer grain) units are deposited over red (coarser grain) units, due to the fault breach. After the fault has breached through, the propagation of the normal fault no longer affects the monocline, thus it starts to erode. The relief in the model exhibits a growing sigmoidal shape where terrigenous clinoforms are deposited. The Wheeler diagram exhibits a diachronous trend, where units with the same lithological properties form at

different times and locations (Nichols, 2009). Deposited sediments (e.g. facies) in the model are prograding, where diachronous units prograde basinward, driven by sediment supply from the gradually steepening slope gradient (e.g. diffusion). This is caused by the evolution of the propagating normal fault that creates more accommodation space over time. Clay, silt, and fine sand have a prograding stacking pattern from about $y = 500$ to 700 m along the section (Figure 6f). The fine sand gradually ceases to deposit at about 720 m whereas the clay and silt sized particles are deposited further into the basin.



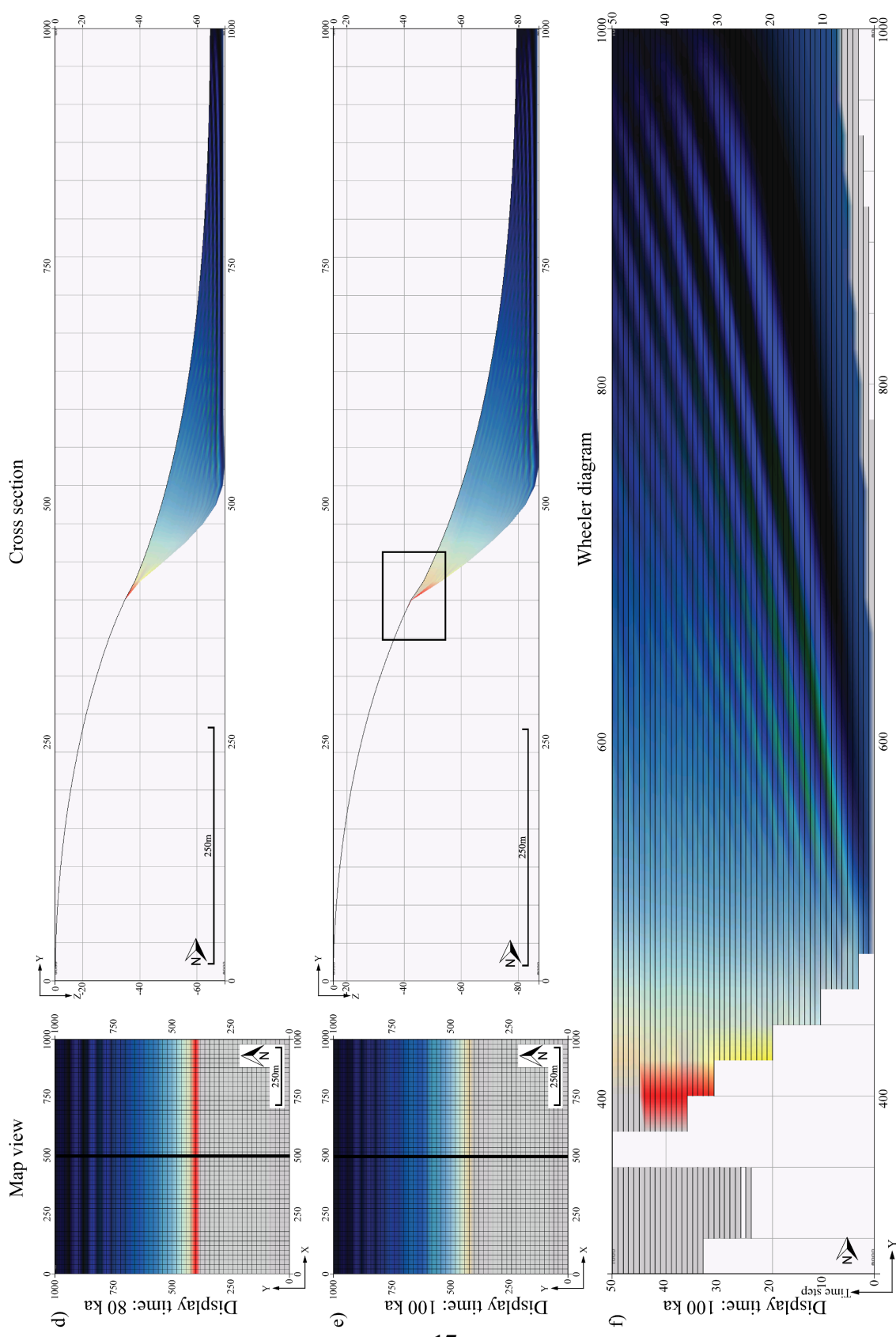


Figure 6: Sequential evolution of the model with constant trishear parameters (K), first as a map view (left), then as a cross-section (right). The model is 3x vertical exaggerated. The model is shown at a) 20, b) 40, c) 60, d) 80, and e) 100 ka. f) Wheeler diagram. The vertical axis is time, and the colours are different facies.

3.1.2 VFS MODEL – VARIATION OF FAULT SLIP ALONG STRIKE

The next models investigate the effects of varying fault slip along strike. This particular model (VFS) has differing fault slip rates along strike as described in Table 3 and Figure 7, where the fault slip rate decreases linearly along strike, and the eastern fault tip has twice as much fault slip as the western tip. During the simulation, the cells in the NW corner of the model remain unaffected from sedimentation.

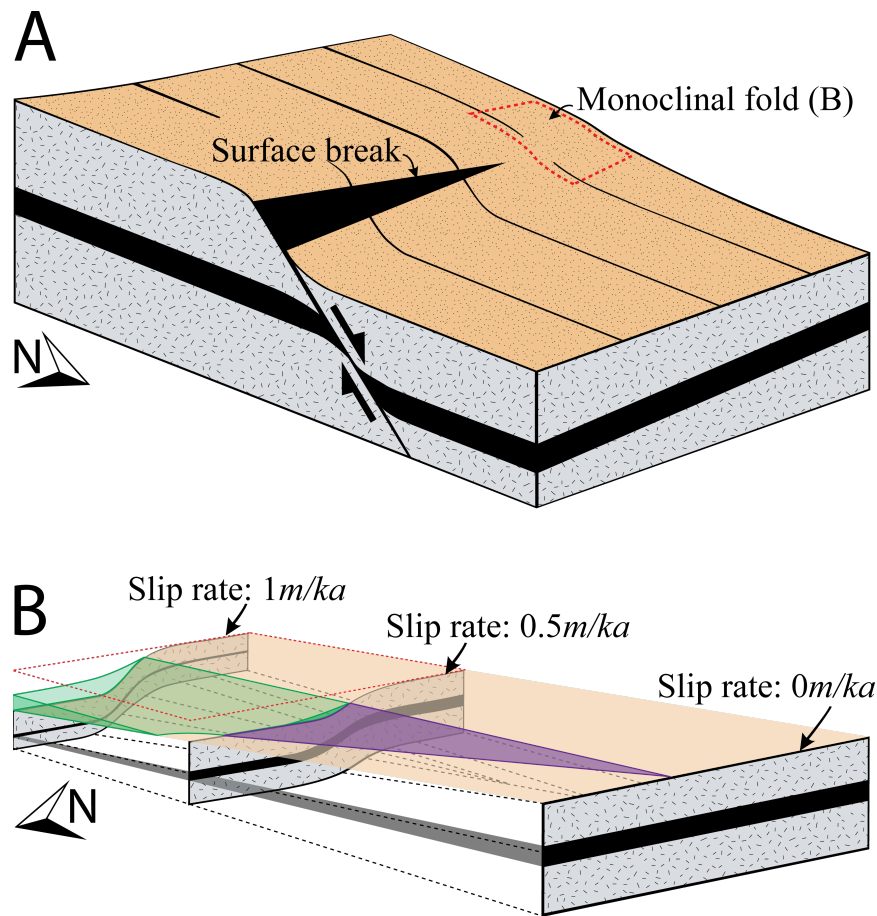


Figure 7: A) Schematic illustration of a normal fault associated with lateral and vertical propagation of fault tip. The block diagram illustrates the behaviour of monoclinial folds along strike (modified from Gawthorpe *et al.*, 1997). The red dashed rectangle indicates the location of B and model VFS. B) Schematic illustration displaying the concept of varying fault slip rate and the extent of the model VFS (red dashed square). The purple area shows where the rest of the sedimentary wedge and the fault tipline would be.

Hence, a planar area develops in the NW corner, progressively dipping towards the NE corner (map view, Figure 10a-e). This holds throughout the simulation, where the hanging wall is gradually tilted, leaving the western side (low fault slip rate) higher than the eastern side (high fault slip rate) (Figs. 7, 8, 9b and 10). A varying fault slip rate along strike results in a wider monocline in the west compared to the east (Figs. 8 and 10). The western fault tip (low slip rate) lies deeper beneath the overlying fold compared to the eastern fault tip (high slip rate). The trishear zone impacts the model differently from west to east. The hanging wall section has a steeper forelimb in the eastern part (high slip rate), relative to a gentler forelimb in the western part (low slip rate) (Figure 8). Fault slip rate variation along strike creates a differential slope gradient. The slope gradient increases to the east, tilting the model eastward (Figs. 7, 9 and 10). In this model, the depocenter is in the NE corner (Figs. 7b and 10), since the tilting leads to more accommodation space in the NE part compared to the NW, resulting in a sedimentary wedge (Figure 9b). Moreover, the main controlling parameters (e.g. fault slip and diffusion) influence the sedimentation and accommodation space. These parameters influence the spatial distribution of the facies, where coarse sediment deposits are more condensed in the west, compared to the east where finer sediments tend to accumulate (Figure 9). The accumulation of coarse sediments in the western part of the model can be an effect of the NE tilting formed by various slip rates since coarser sediments do not transport as far as finer sediments (Figs. 9 and 10, Wheeler diagram). Various slip rates cause the western part to be uplifted relative to the eastern part of the model, thus there is more erosion in the west (Figure 9b). The wider area affected by the trishear zone in the western part (Figure 8) can also affect the accumulation of coarse sediments, compared to the eastern part where the monocline is narrower. Sediment accumulation is higher in the east due to a steeper slope gradient (Figs. 7, 8 and 10). Along strike (Figure 9), the general deposition of sediments displays an increasing accumulation towards the east (high fault slip rate), similar to the coloured areas in Figure 7.

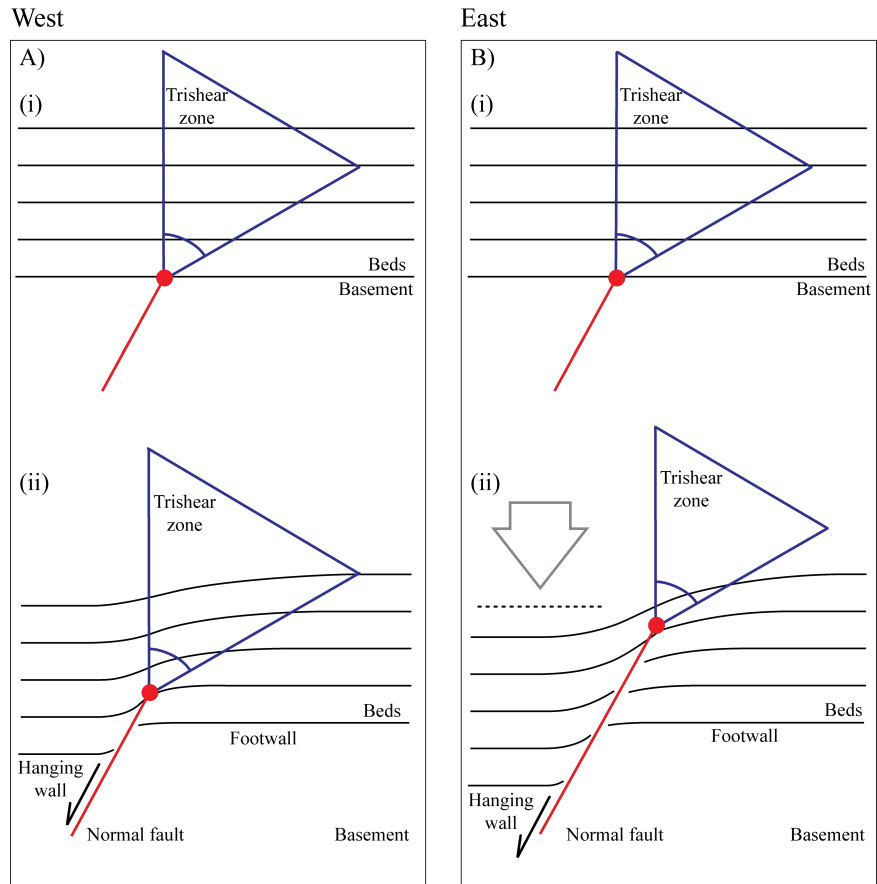


Figure 8: Cross sections showing the effect of various slip rates at opposite fault tips. A) Western fault tip with slip rate = 0.5 m/ka. B) Eastern fault tip with slip rate = 1 m/ka. In both cases, (i) and (ii) are the initial and final stage, respectively. Dashed line in the final stage of B indicates the hanging wall elevation. The model has $P/S = 2$ and trishear angle = 60° .

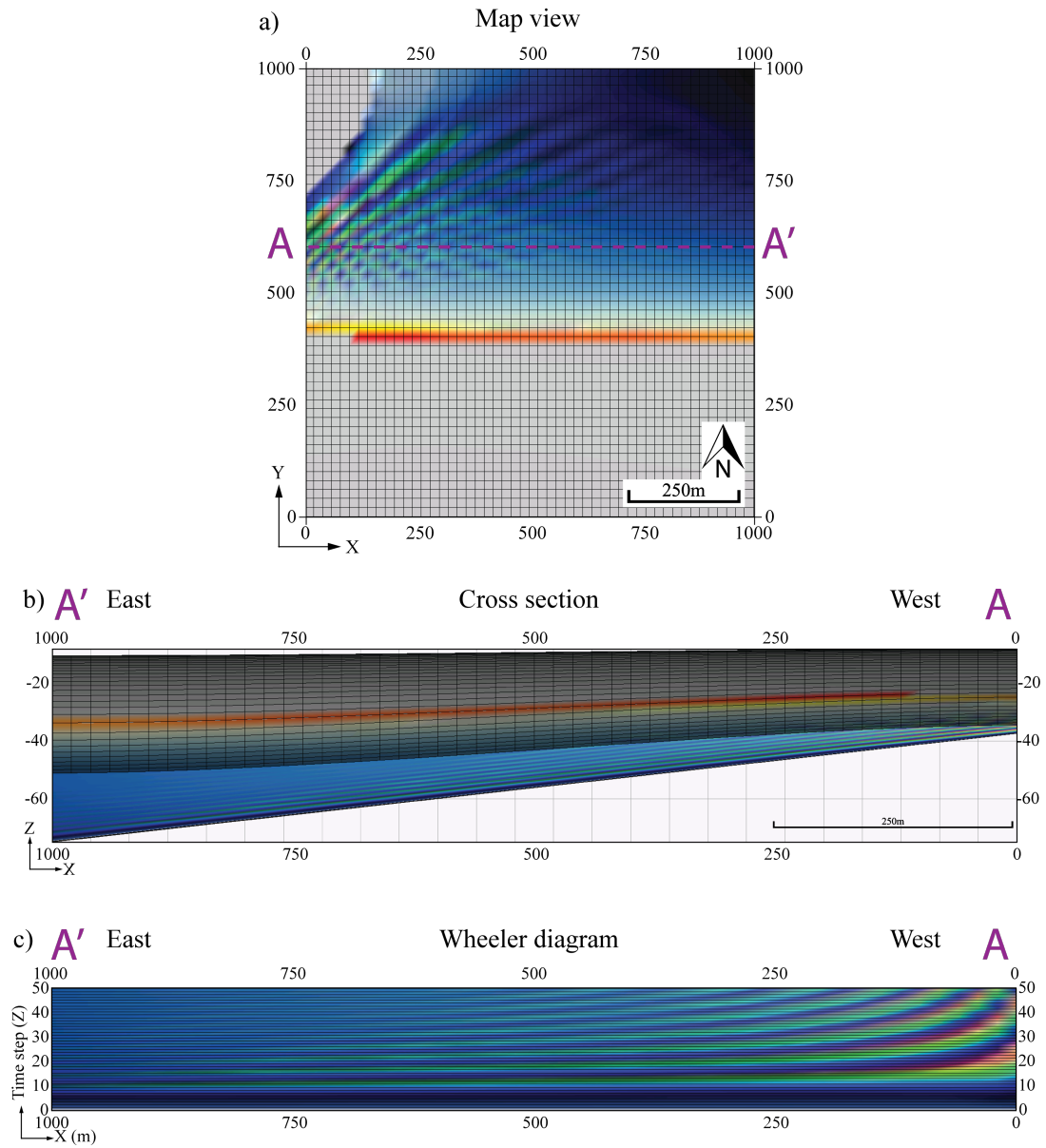
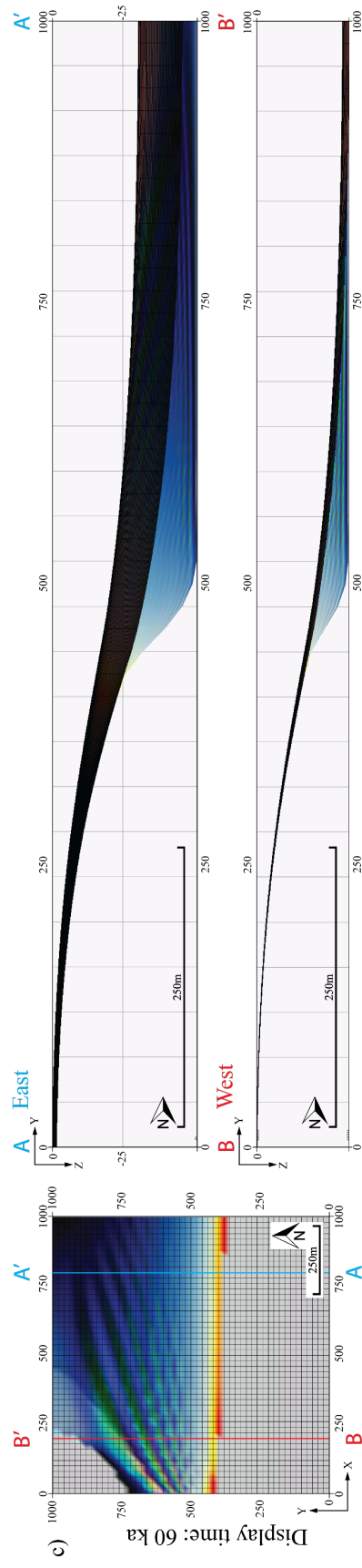
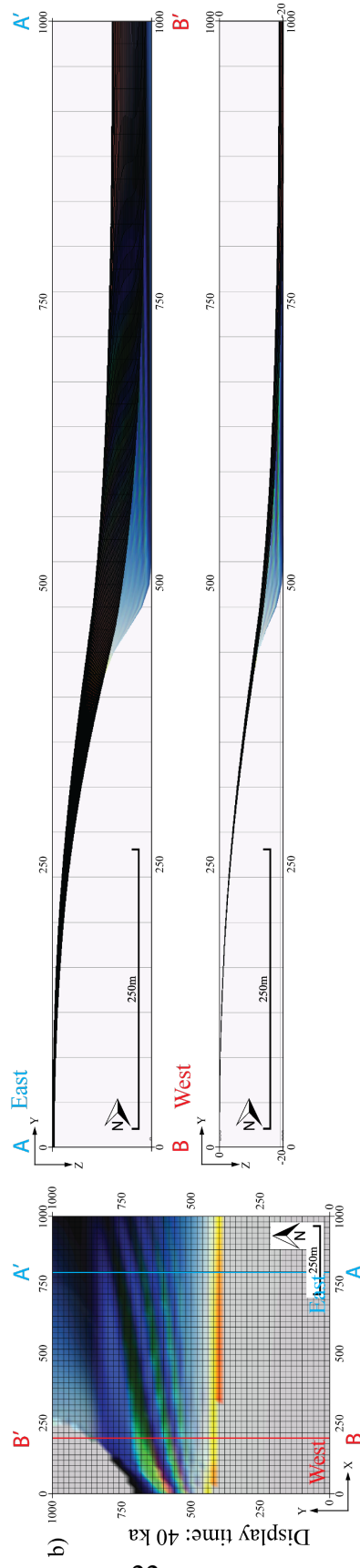
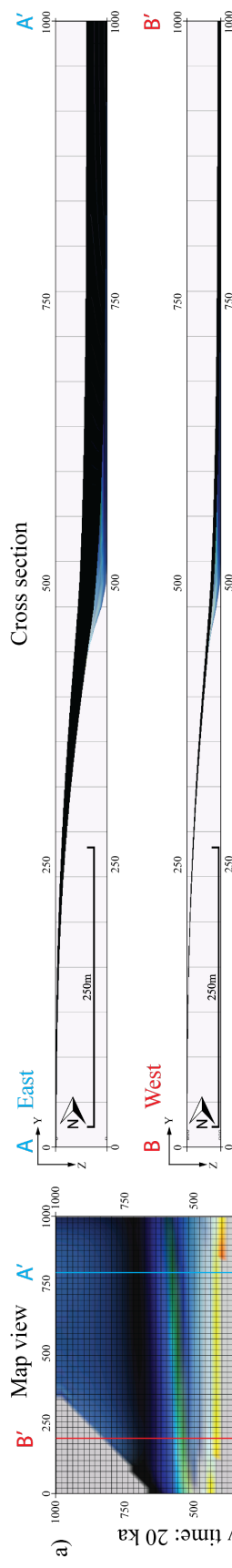
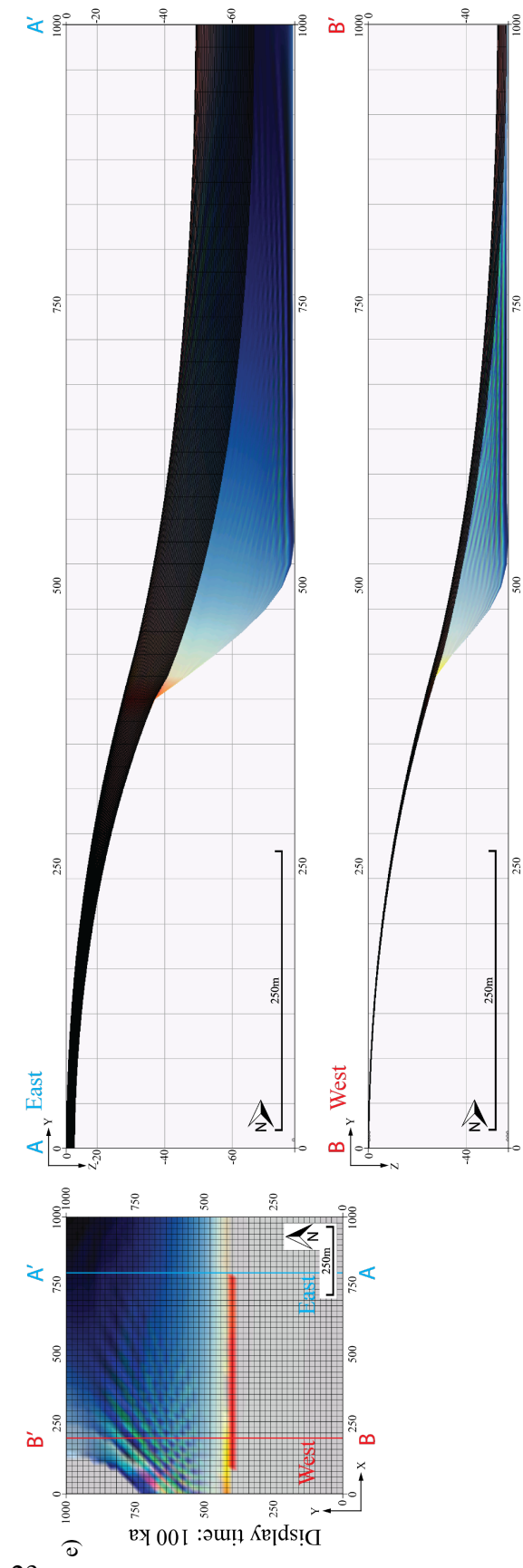
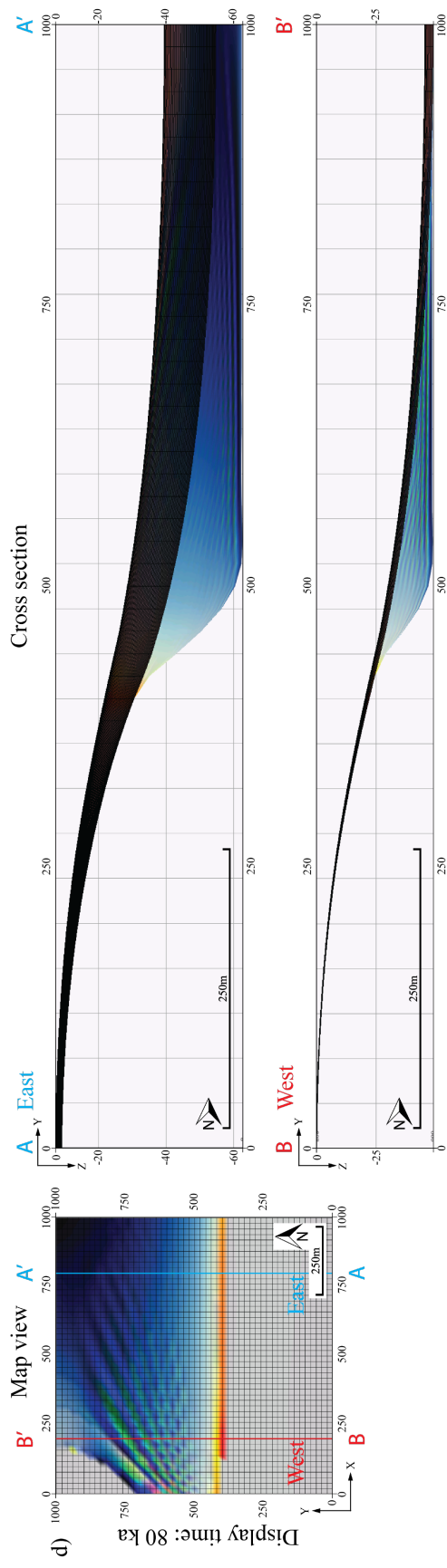


Figure 9: Along strike cross section and Wheeler diagram of VFS model at 100 ka. a) Map view showing the location of the cross section and Wheeler diagram ($y = 600$). b) Cross sections displaying the eastern tilting of the model, leading to sediments depositing as a wedge. c) Wheeler diagram showing the condensation of coarse sediments (green and red) in the west compared to the east.





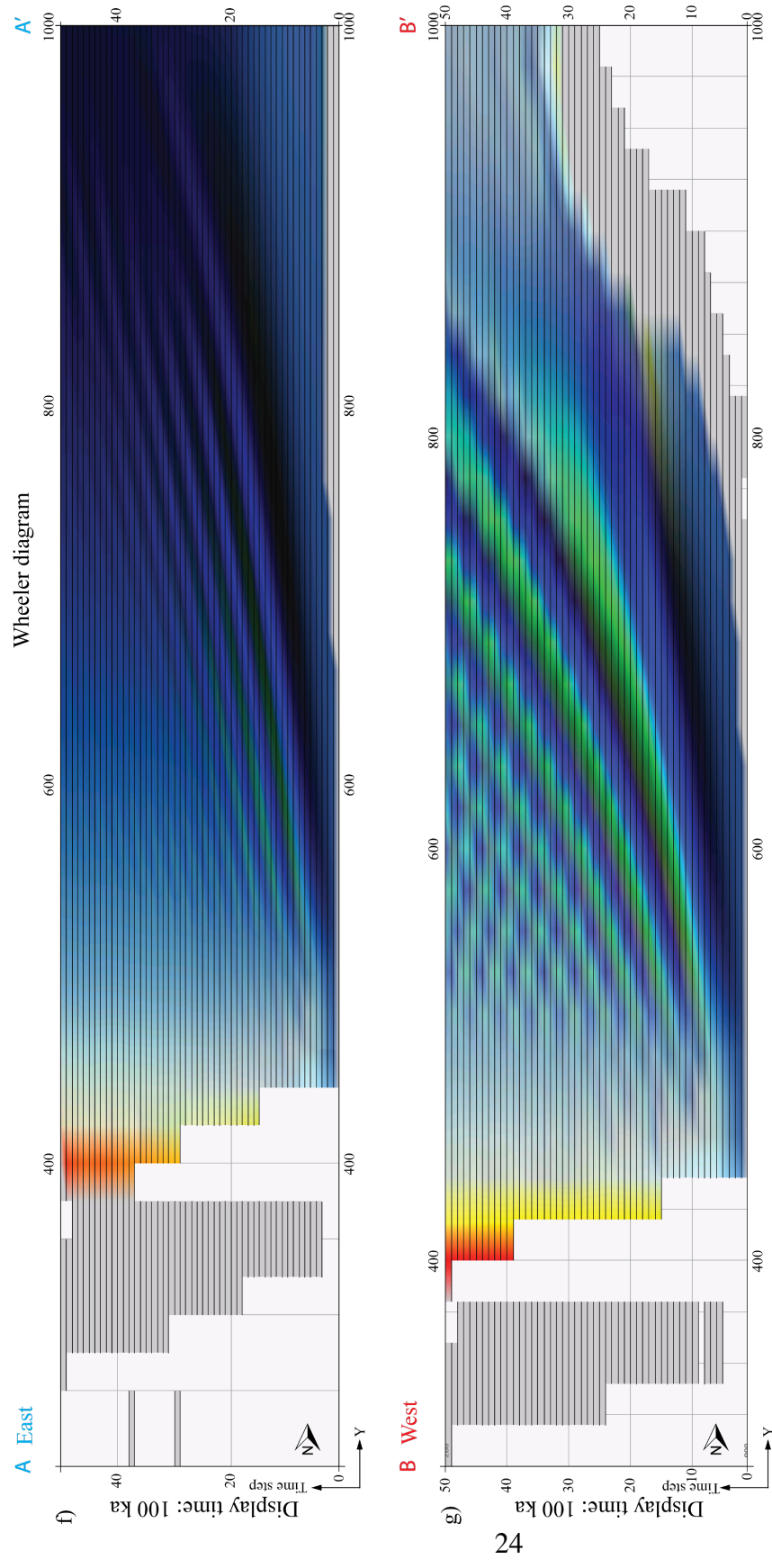


Figure 10: Sequential evolution of the model with various slip rates along strike (VFS), as map view (left) and N-S cross-sections (right). Blue A-A' is the eastern (high slip rate) section at $x = 800$ m, whereas red B-B' is the western section (low slip rate) at $x = 200$ m. The model is 3x vertical exaggerated. The model is shown at a) 20, b) 40, c) 60, d) 80, and e) 100 ka. f and g) Wheeler diagrams along the same sections. The vertical axis is time, and the colours are different facies.

3.1.3 VTA MODEL – VARYING TRISHEAR ANGLE ALONG STRIKE

The next model (VTA) investigates the effect of varying the trishear angle along strike. The trishear angle at the western fault tip is set to an angle of 100° , while the eastern fault tip has a trishear angle of 40° (Table 3 and Figure 11). The eastern part of the model experiences a narrower trishear zone. This leads to a decrease in the wavelength of the monocline and a steeper forelimb (Figs. 11 and 12). The western part of the model is influenced by a broader trishear zone leading to an increase in the wavelength of the monoclinal fold, hence gentler forelimb (Figs. 11 and 12).

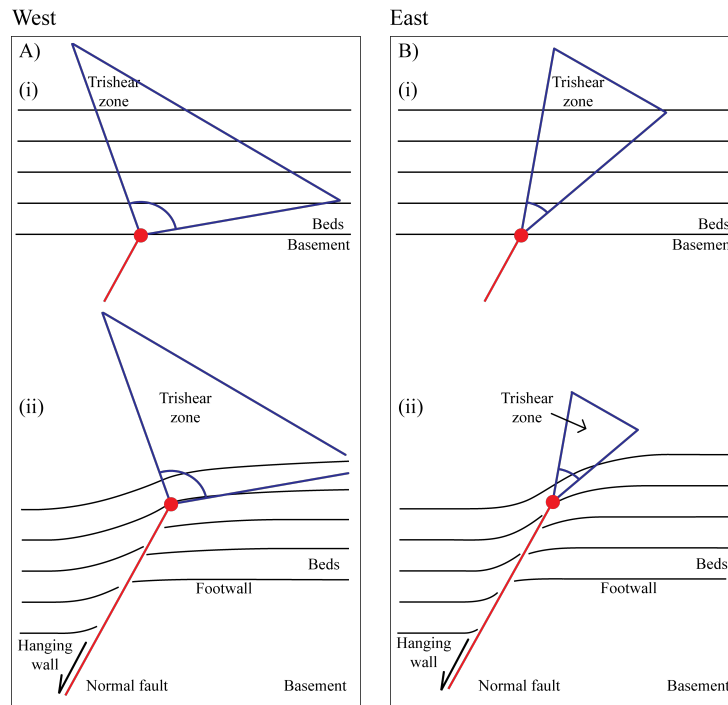
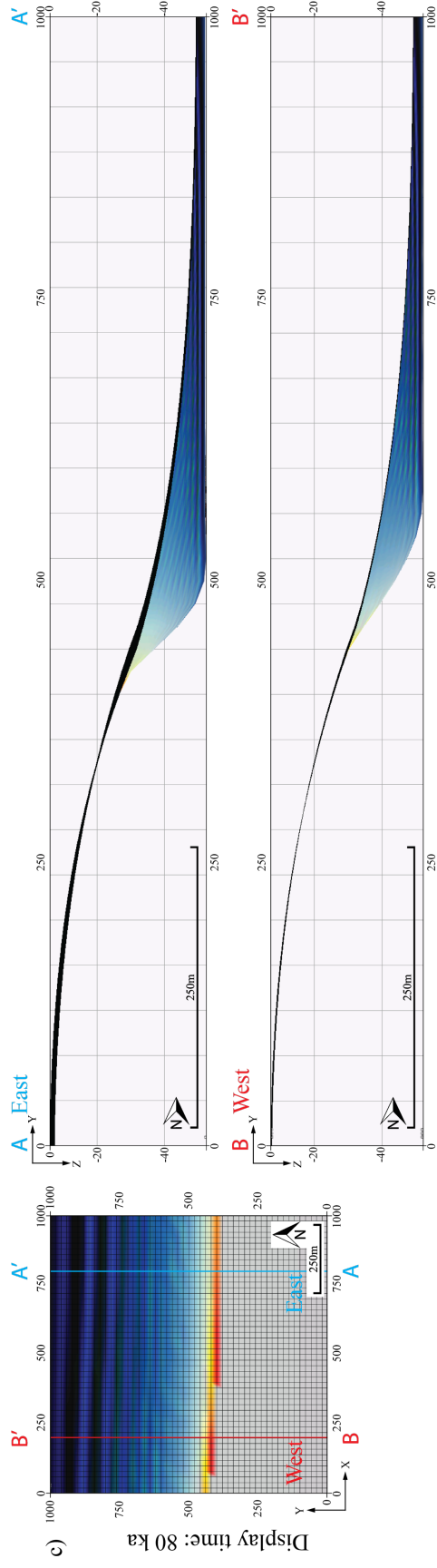
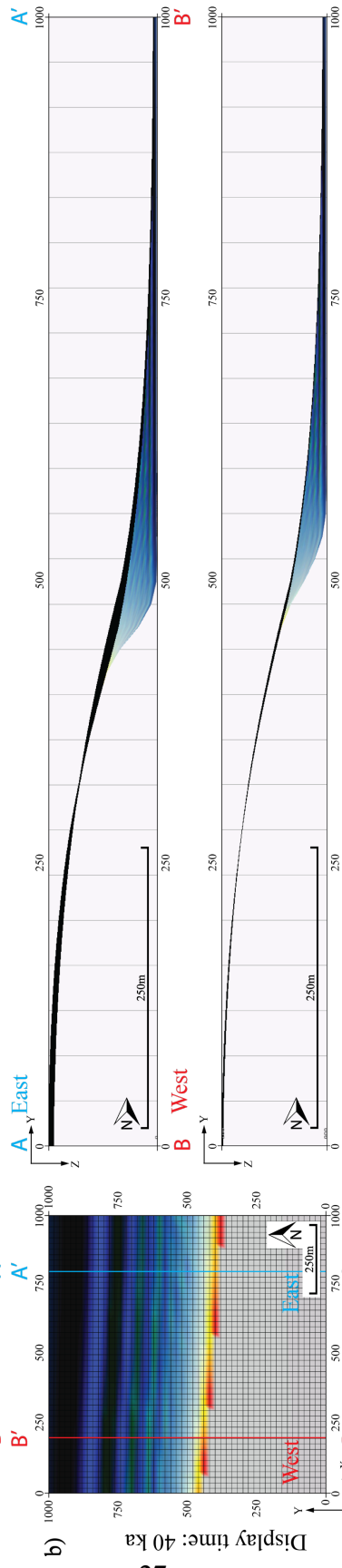
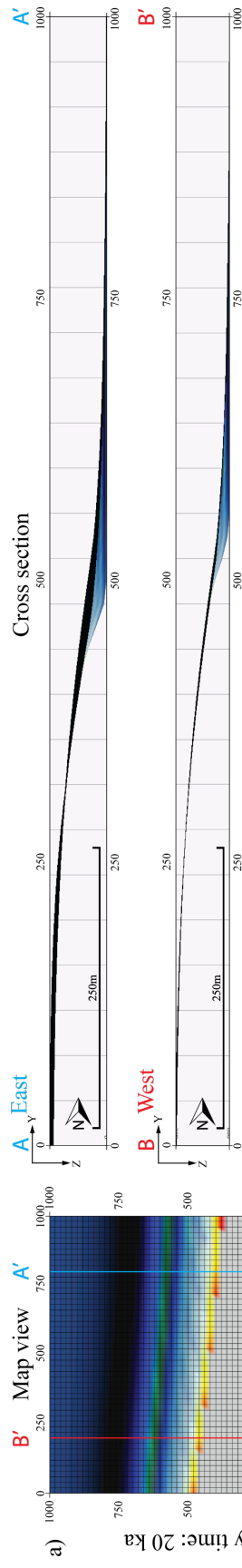


Figure 11: Cross sections showing the impact of different trishear angles at opposite fault tips. A) Western fault tip with a trishear angle of 100° . B) Eastern fault tip with trishear angle of 40° . In both cases (i) is the initial stage, and (ii) is the final stage. The model has fault slip rate = 1 m/ka, and P/S = 2.

A larger trishear angle (west) leads to a broader and less intense zone of deformation, conversely, a smaller trishear angle (east) results in a narrow and more intense zone of deformation (Gawthorpe and Hardy, 2002). Notice the black area covering the eastern

cross-section A-A' in Figure 12a-c. This represents the difference in monoclinical fold geometry between sections A-A' and B-B'. Through the simulation, the slope gradient differs along strike as result of different trishear angles at the fault tips. Going from a gentle slope in the western part, gradually to a steeper slope in the eastern part, as demonstrated in Figures 11 and 12. During the simulation, the coarse facies are deposited near the slope break in a diagonal east – northwest trend (map view, Figure 12a-c). This can also be observed in the cross sections in Figure 12a-e. Hence, there is offset of the slope break in the north (y) direction, where the western slope break is more distal than the eastern slope break. The western slope break gradually becomes more proximal during the simulation. Over time, the variation in monoclinical fold geometry along strike decreases and almost completely disappears at the end of the simulation (cross-section in Figure 12e). Both the trends of diagonal slope break and monoclinical fold geometry tend to cease at the same time, and a surface break is visible, meaning that the fault has breached the monocline (Figure 12e). The variation in trishear angle controls the deformation zone, which widens more up section in the west than in the east. Thus affecting the slope gradient, and resulting in a steeper forelimb in the eastern section. Along the dip direction, a gentler slope in the west influences the depositional morphology in the sense of a more elongated lens shaped unit than in the east (Figure 12e). The spatial distribution of facies follows the diagonal trend of the slope break at first, prograding basinward (map view, Figure 12a-c). Figure 12 c) to e) in cross section, shows the facies (e.g. fine sand) tend to align in an SW - NE direction. The Wheeler diagrams (Figure 12f-g) demonstrate that facies (e.g. fine sand) in the western section prograde further into the basin compared to the eastern part. The Wheeler diagram also shows that coarser facies retrograde more in the section of the west than in the eastern section. A Wheeler diagram along strike would show facies prograding eastward, especially in the area of the slope toe (e.g. fine sand). For the western section, this would be at $y = 600$ m, and for the eastern section at around $y = 500$ m.



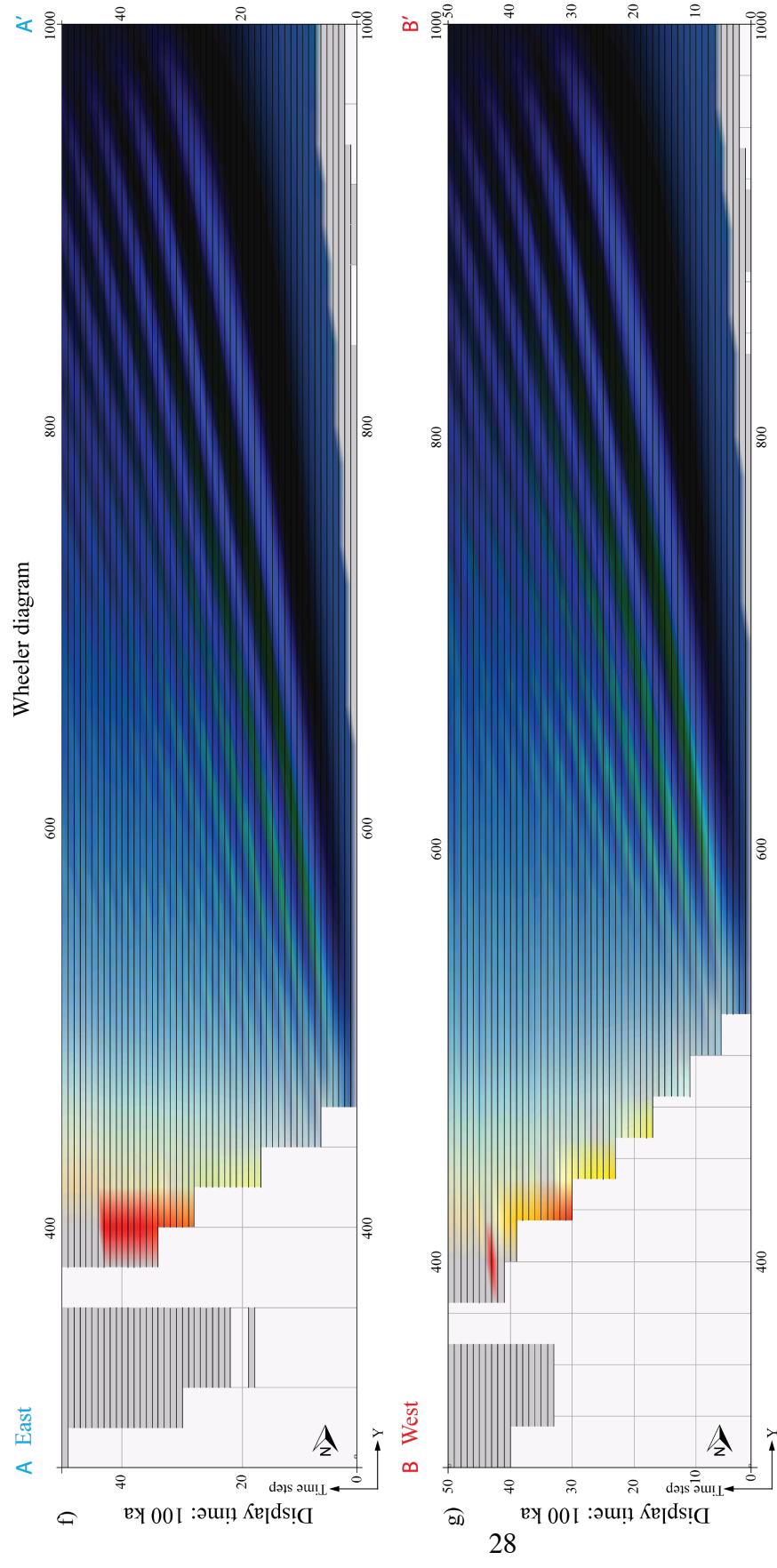
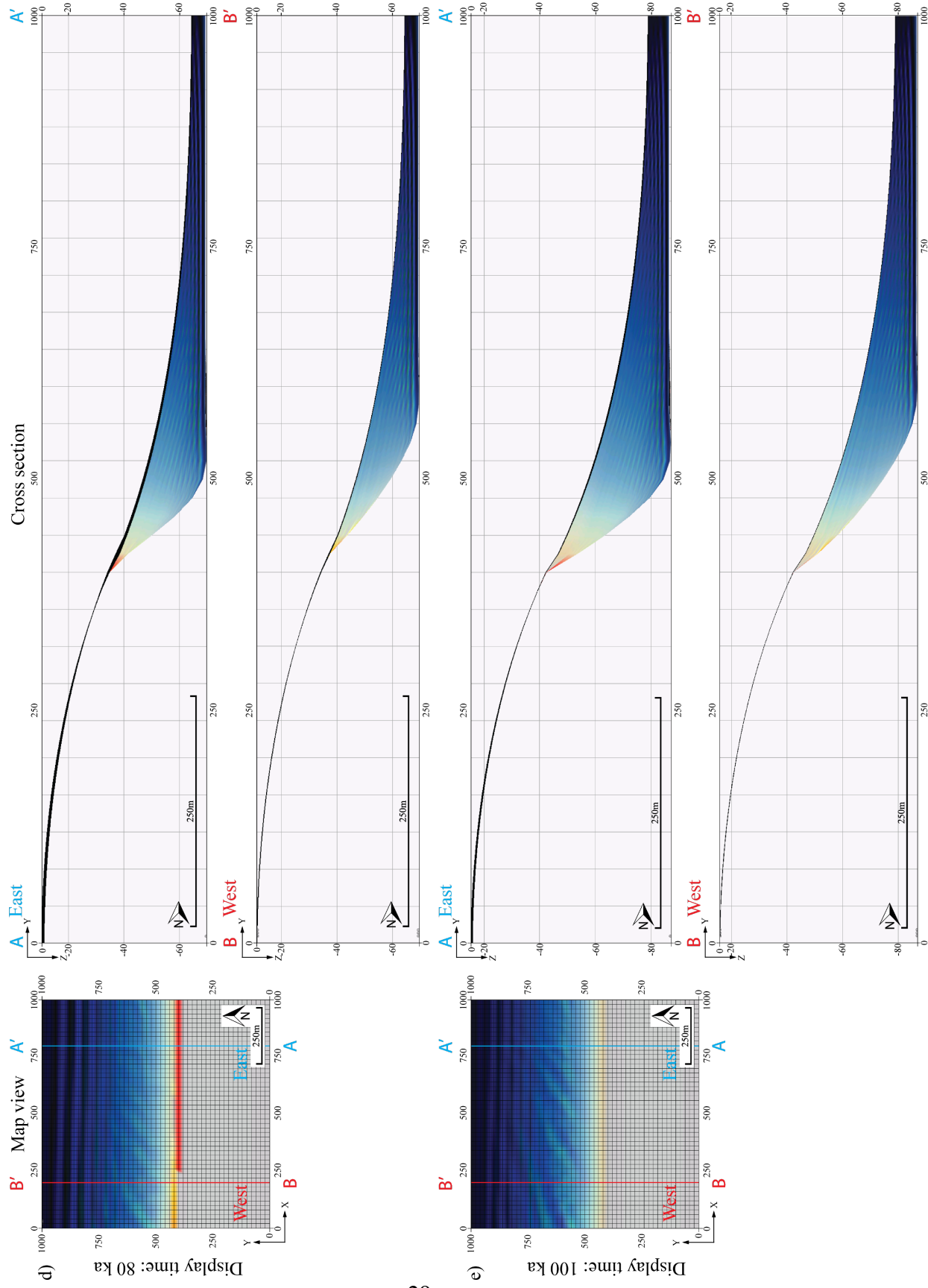


Figure 12: VTA model with variation in trishear angle. Western fault tip has a trishear angle of 100° , while eastern fault tip has a trishear angle of 40° . The model is 3x vertical exaggerated. Map view and eastern (A-A') and western (B-B') sections are shown at a) 20, b) 40, c) 60, d) 80, and e) 100 ka. f and g) Wheeler diagrams along the same sections. The vertical axis is time, and the colours are different facies.



3.1.4 VPS MODEL – VARYING P/S ALONG STRIKE

The next model investigates the effect of a linear variation of P/S along the fault (VPS). Hence, the east fault tip is assigned P/S ratio of 1, and the west fault tip is assigned a P/S of 4 (Table 3). With a lower P/S ratio, the eastern section develops a tight monocline with steep forelimb, where the fault tip is deeper than on the western section (Figs. 13 and 14). Higher P/S ratio in the western section, results in a more open monocline, a gentler forelimb, and breaching of the monocline at an early stage (Figs. 13 and 14). Along strike variations of P/S impact the migration of the trishear zone, and in this case breaching through the western section. During the simulation, the coarser facies start depositing in the west (high P/S), and gradually move eastward (low P/S) along the slope break (map view, Figure 14a-e). This is due to the linear variation of P/S along strike, which makes the western fault tip propagates more rapidly than the eastern fault tip. The black area covering the eastern cross section A-A' in Figure 14a-e represents the difference in fold geometry between section A-A' and B-B'. In the western section, the propagating fault breaches the monocline at 60 ka (map view, Figure 14c), and in cross section view it is easy to recognize the breach

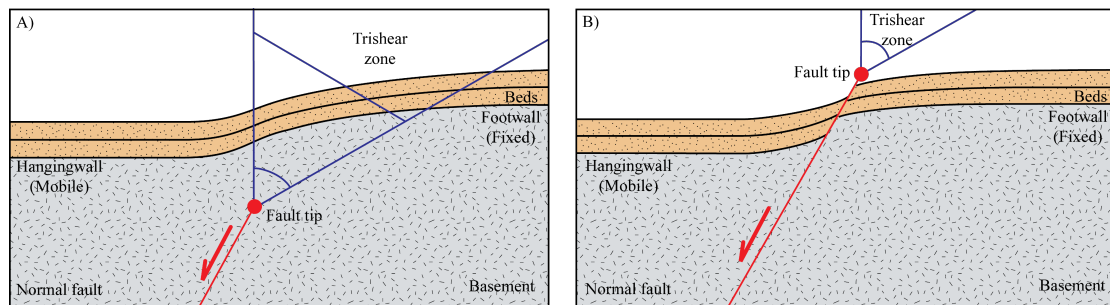
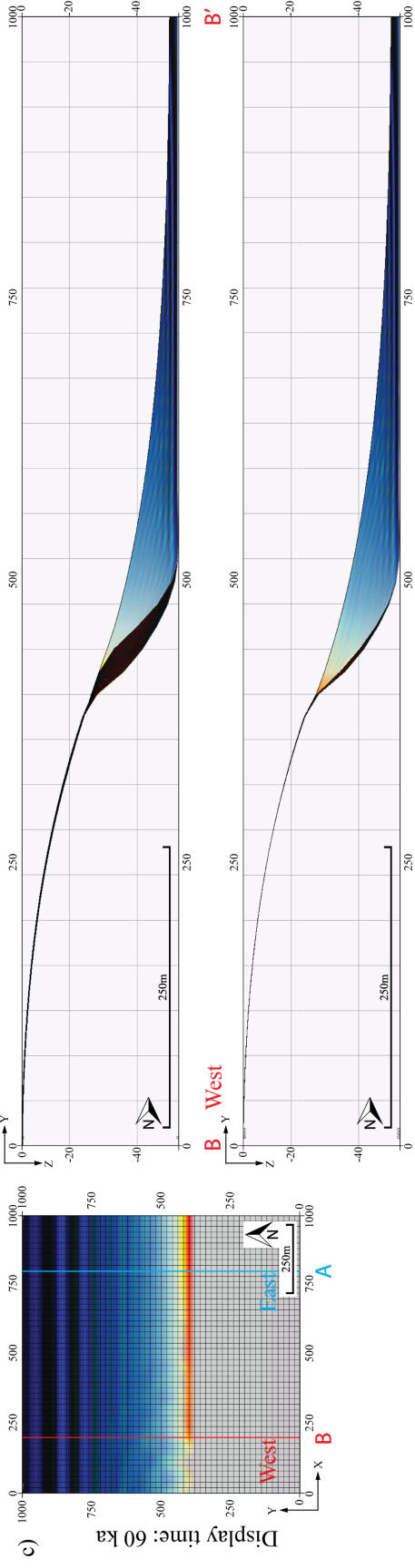
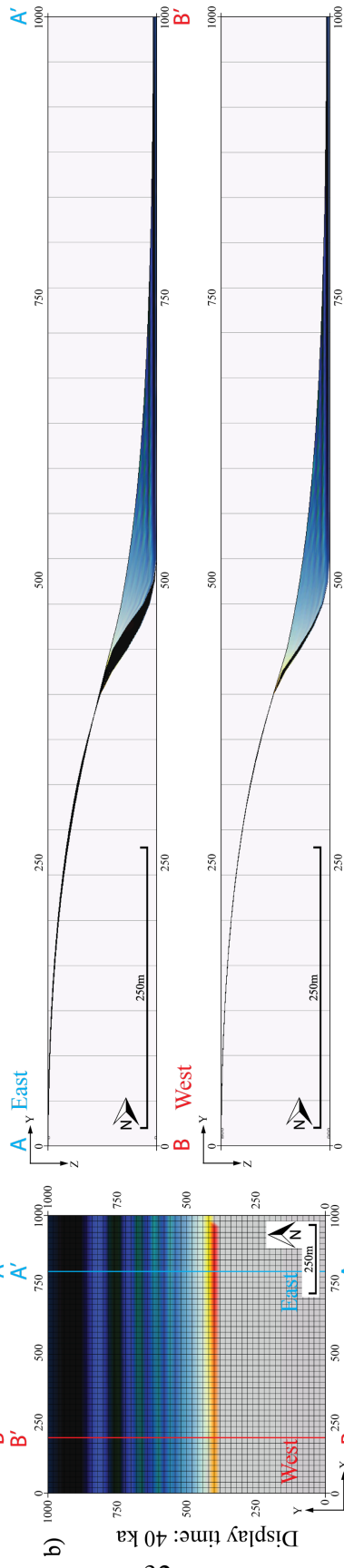
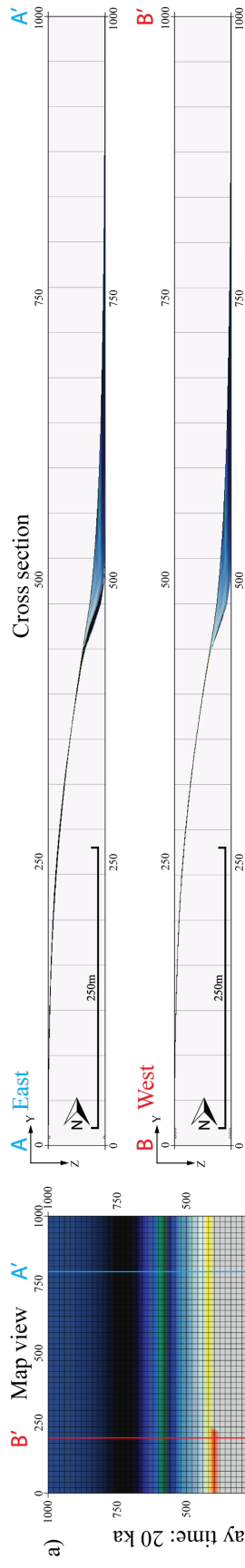
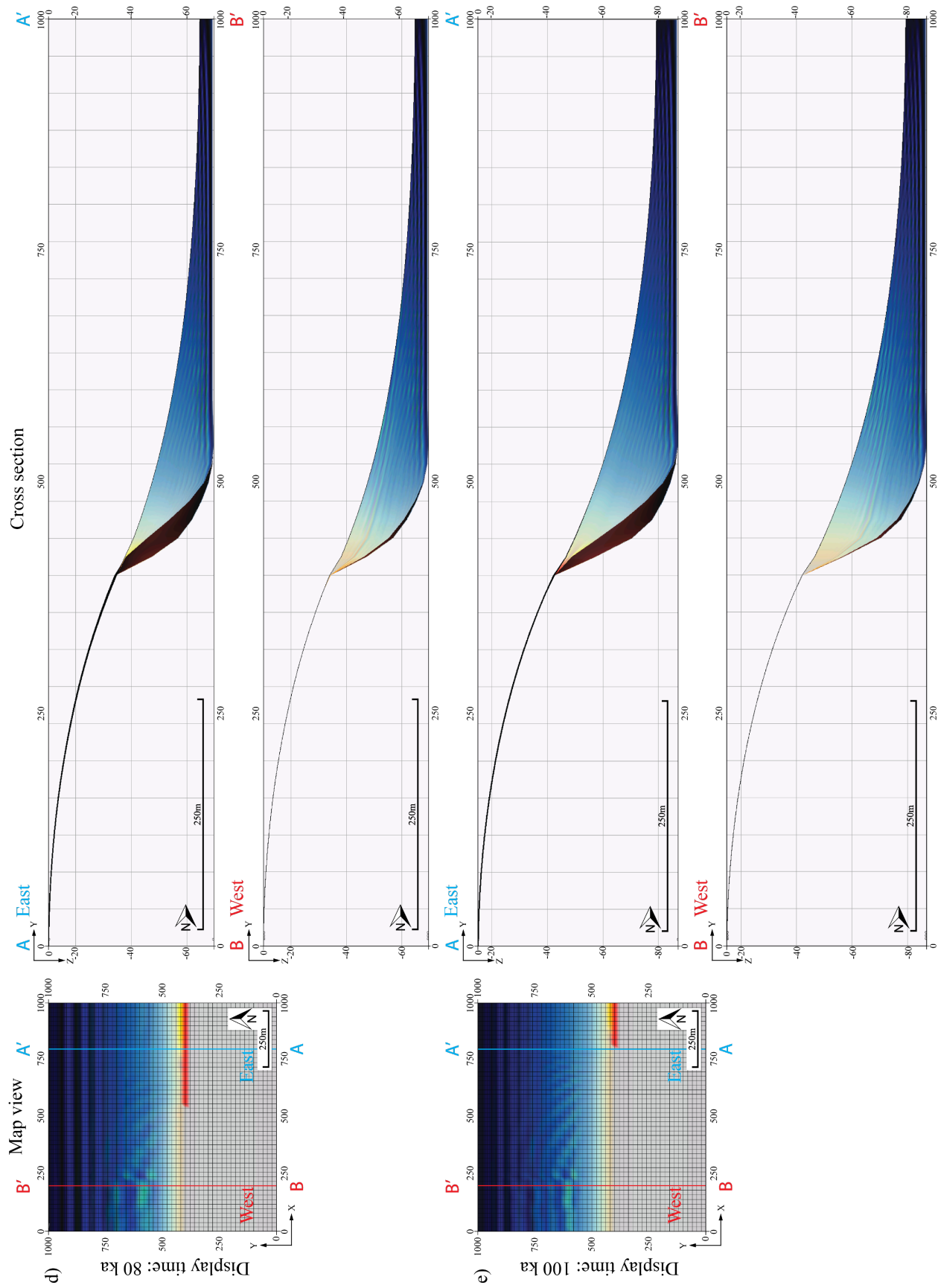


Figure 13: Schematic illustration displaying different P/S ratios on propagating normal fault, with a ramp of 60° and trishear angle = 60°. A) P/S = 1, tighter monocline with steep forelimb. B) P/S ratio = 4, broader monocline and fault breaching the fold.

as a shift in facies near the slope break (cross section, Figure 14d-e). In the west, coarser facies (e.g. red), at a given time, deposit more distal than older deposits. This is better demonstrated in the western Wheeler diagram (Figure 14g), where first a progradational trend is observed from cycles 1-30. From around cycle 30 (60 ka), the facies display a rapid retrograding trend when the monocline is breached, and further in time, the facies again display a prograding trend. After the fault breaches the monocline, a radial pattern is shown by coarser facies going from west to east (Figure 14c-e).





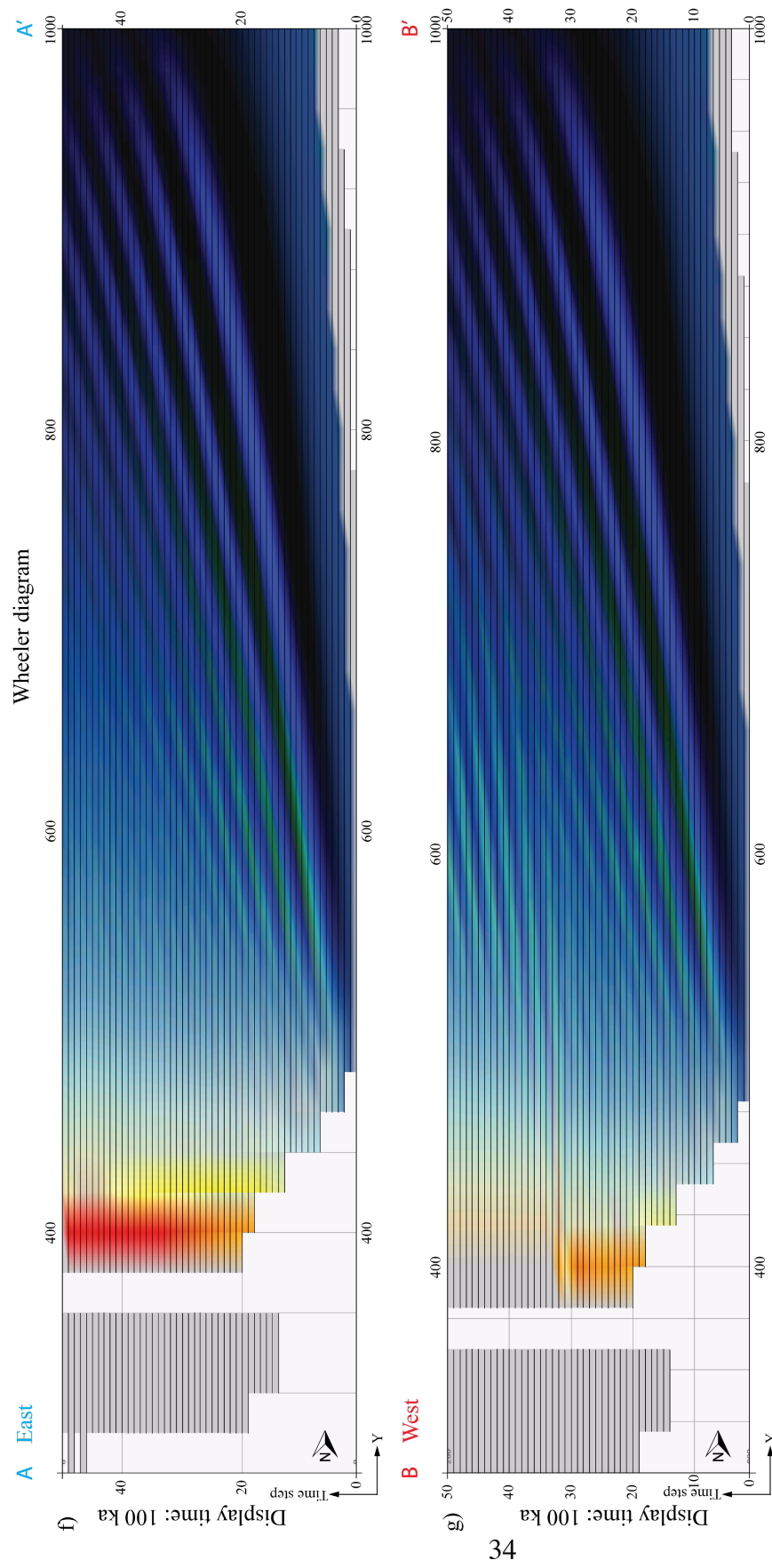
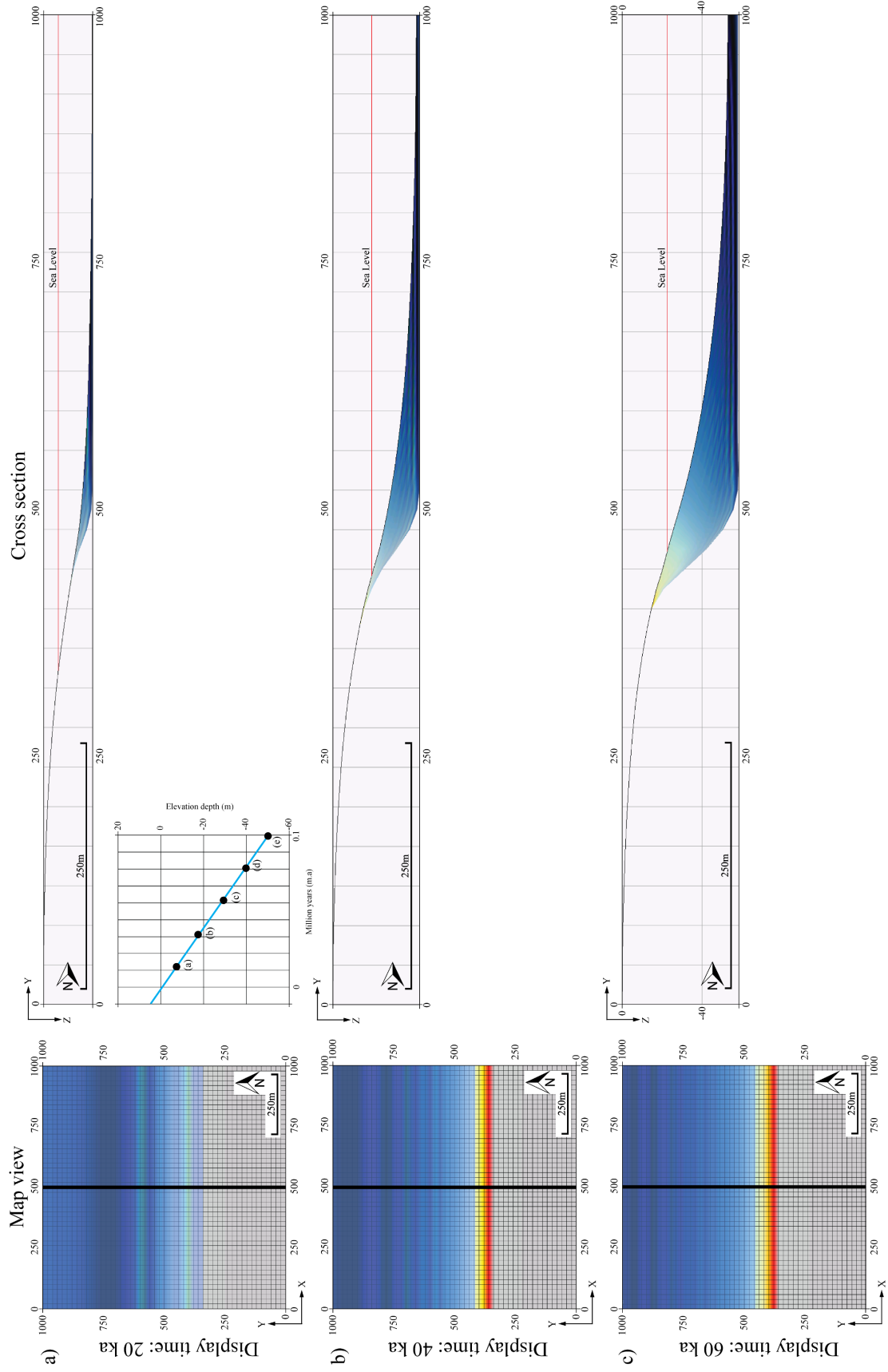


Figure 14: VPS model with a linear variation of P/S along the fault. The east fault tip has a $P/S = 1$, and the west fault tip has a $P/S = 4$. The model is 3x vertical exaggerated. Map view and eastern (A-A') and western (B-B') sections are shown at a) 20, b) 40, c) 60, d) 80, and e) 100 ka. f and g) Wheeler diagrams along the same sections. The vertical axis is time, and the colours are different facies

3.1.5 SLD

MODEL – SEA LEVEL DROP

The next model investigates the results from a linear sea level drop with no variation of trishear parameters along strike (Table 3). This model examines the strata geometries formed as result of sea level drop. The sea level curve used in this model starts at zero elevation at 0 and drops linearly 50 m after 100 ka (Figure 15a). During the simulation, as sea level drops, it bypasses the slope top, which leads to an increase in sediment supply. In response to this, accommodation space becomes limited, and sediments are forced to build into the basin (Figure 15b-e). This is similar to a forced regression, where sedimentation is affected by a shift in the shoreline. Due to the drop in sea level, the shoreline change from proximal to distal, providing a greater sediment supply when a larger area of the slope becomes exposed and prone to erosion, resulting in broader clinoforms and a subaerial unconformity (Figure 15b-e). As a result of this, coarser facies (yellow to orange) display progradation (Wheeler diagram, Figure 15f) with downstepping geometries (cross section Figure 15e). In reaction to a drop in sea level, more sediments become exposed and can be eroded, resulting in a thicker sequence of growth-strata compared to the other models (Figure 15e).



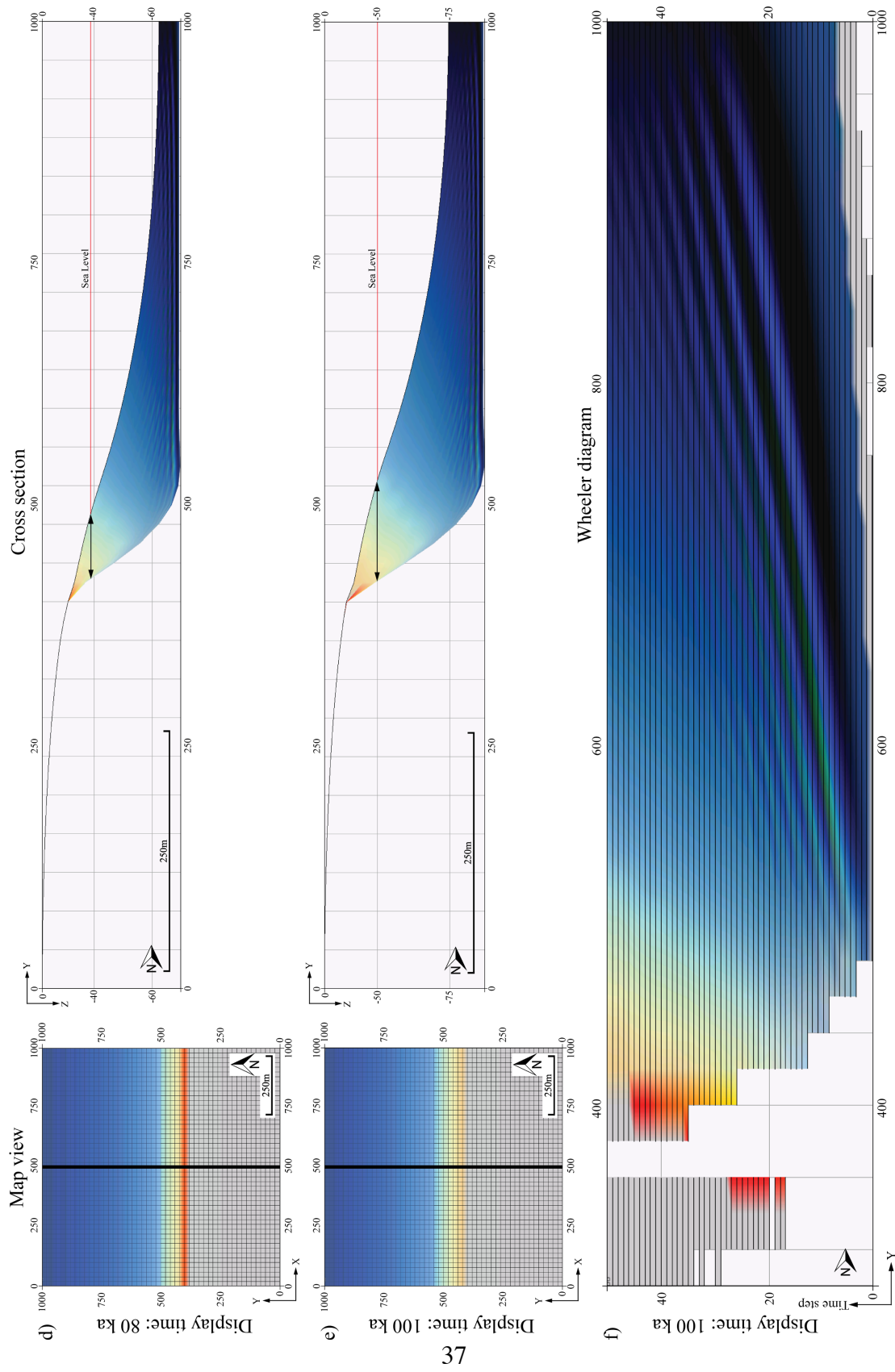


Figure 15: SLD model with linear sea level drop. The model is 3 x vertical exaggerated. Map view and N-S cross section are shown at a) 20, b) 40, c) 60, d) 80, and e) 100 ka. Black arrow in d) and e) indicates growth. f) Wheeler diagram along the same section. The vertical axis is time, and the colours are different facies.

3.1.6 SINRISE MODEL – SINUSOIDAL RISE OF SEA LEVEL

The last model investigates the interplay of a more realistic variation in sea level. The model uses a sinusoidal curve with an amplitude of 25 m and a period of 100 ka (Figure 16a). At the beginning of the simulation, the relative sea level (RSL) is not visible (Figure 16a). The RSL rise manifest after 32 ka, just before Figure 16b, and RSL continues to rise until 76 ka just before Figure 16c. RSL then falls for the remainder of the simulation. In an effort to better interpret the results of this model, a sequence stratigraphic approach was used. Successions of genetically related parasequences were interpreted forming a characteristic stacking pattern (AAPG Methods in Exploration 7, 1990). The stacking pattern includes aggradation, progradation, and retrogradation parasequence sets. The system tracts were defined using significant unconformities (Van Wagoner *et al.*, 1988). Between 20 and 40 ka (Figure 16a-b), the model goes from an RSL fall to an end of a regression. This is the lowstand system tract (LST), where the RSL is starting to rise. In response to the LST, RSL bypasses the slope break, the coastline shifts landward, and sediments forestep and form aggrading clinoforms (Catenuanu *et al.*, 2011). From 40 and 60 ka (Figure 16b-c), the model is in a transgressive phase where RSL is rising, which is referred as a transgressive system tract (TST). The coastline shifts landward and sediments retrograde (e.g backstepping) (cycle 20, Figure 16f). The accommodation space outpaces the sedimentation rate (Catenuanu *et al.*, 2011). Retrogradational clinoforms thickening landward form. Between 60 to 80 ka (Figure 16c-d), the model is in a highstand phase where accommodation increases slowly, leading to normal regression driven by sediment supply. Normal regressions occurring after transgressions are referred to as a highstand system tract (HST). This indicates that over time, the rates of progradation increase and aggradation rates decrease (Catenuanu *et al.*, 2011). This is demonstrated in the Wheeler diagram (Figure 16f). From 80 - 100 ka (Figure 16d-e), the model is in a falling-stage system tract (FSST), which leads to a forced regression. RSL fall drives sediments to prograde and the coastline to move

basinward (Catenuanu *et al.*, 2011), as demonstrated in the Wheeler diagram (Figure 16f). In the final steps of the model, the RSL does not bypass the slope break again, it stops at elevation 0 m.

For a longer simulation time (e.g. 200 ka), the RSL would bypass the slope break and the model would get a similar response as the previous SLD model regarding the sediments building basinward. The influence of eustatic sea level variations upon continuous deformation (propagating normal fault) can result in more complex growth-strata, where the change in RSL dominate the sedimentation in given time intervals.

Furthermore, the effects of the amplitude of sea level variations were explored and are displayed in figure 17. This figure shows the influence of a sinusoidal sea level curve with twice the amplitude as before (50 m). Regarding the system tracts, the two models share similarities to a certain extent. The increased amplitude of the sea level curve in Figure 17 amplifies the end result. The change in RSL influences more the sedimentation, whereas the RSL falls and rise more rapidly, compared to the model with lower amplitude. In response to a more rapid RSL rise above the margin, the coastline shifts further landward in a shorter period of time. Onlap of thicker proximal (e.g. coarse) facies over (older) distal facies (e.g. fine) becomes more clear, as demonstrated in the cross section of Figure 17 a below the transgressive surface. Due to a shift in coastline landwards, a thicker part of the TST unit terminates at a higher elevation than in the other model with a lower amplitude of sea level variation (Figure 17). When an RSL rise occurs in nature, a ravinement surface (transgressive surface) is produced due to erosion and reworking of former sediments. In the model with high amplitude (Figure 17), a more vivid colour range appears at the boundary TS between the LST and TST. This can be an indication of former sediments being eroded and reworked at that particular time. In the Wheeler diagram, blank sections representing erosion are present at the same time interval (Wheeler diagram, cycle 12-16, Figure

17b). A fining upwards trend from TS to MFS is more distinct in the model with higher amplitude of the sea level curve (Figure 17a). In general, the two figures have similar parasequences, but they are more distinct in Figure 17.

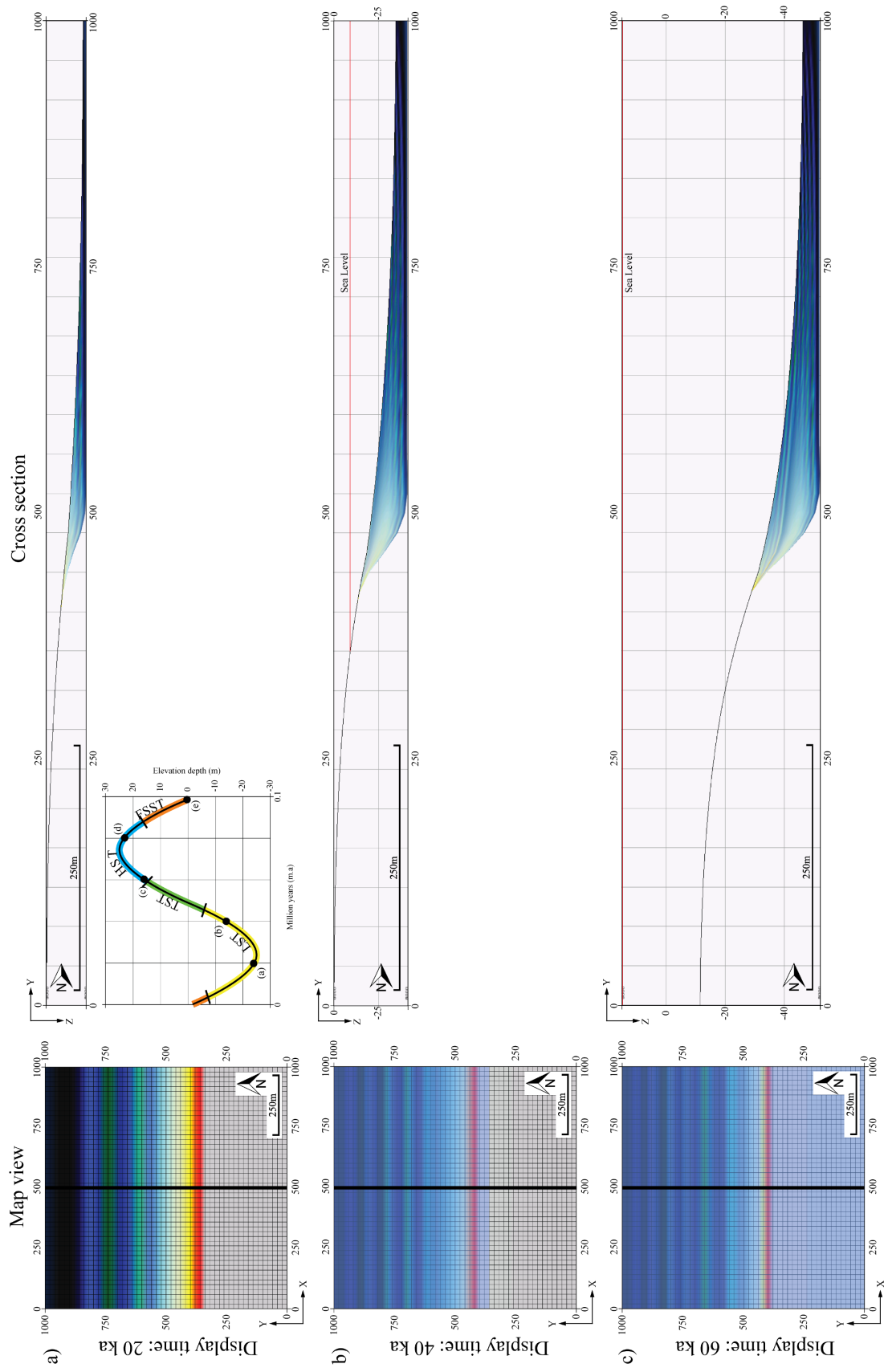
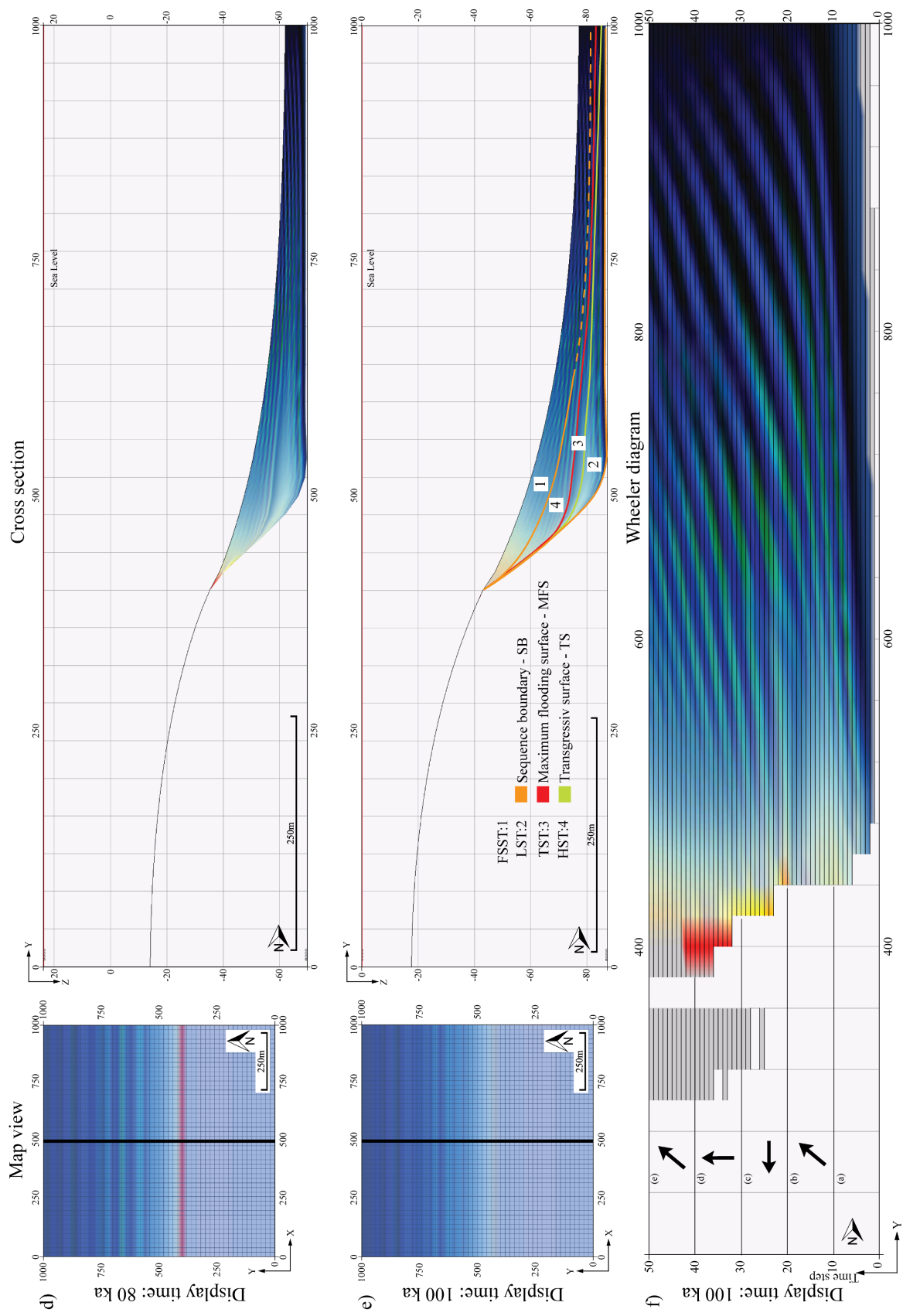


Figure 16: Sinrise model with a sinusoidal sea level curve of 25 m amplitude. The model is 3x vertical exaggerated. Map view and N-S cross section are shown at a) 20, b) 40, c) 60, d) 80, and e) 100 ka. e) contains a sequence stratigraphy interpretation. f) Wheeler diagram along the same section. Black arrows represent (from bottom to top) aggradation, retrogradation, and progradation.



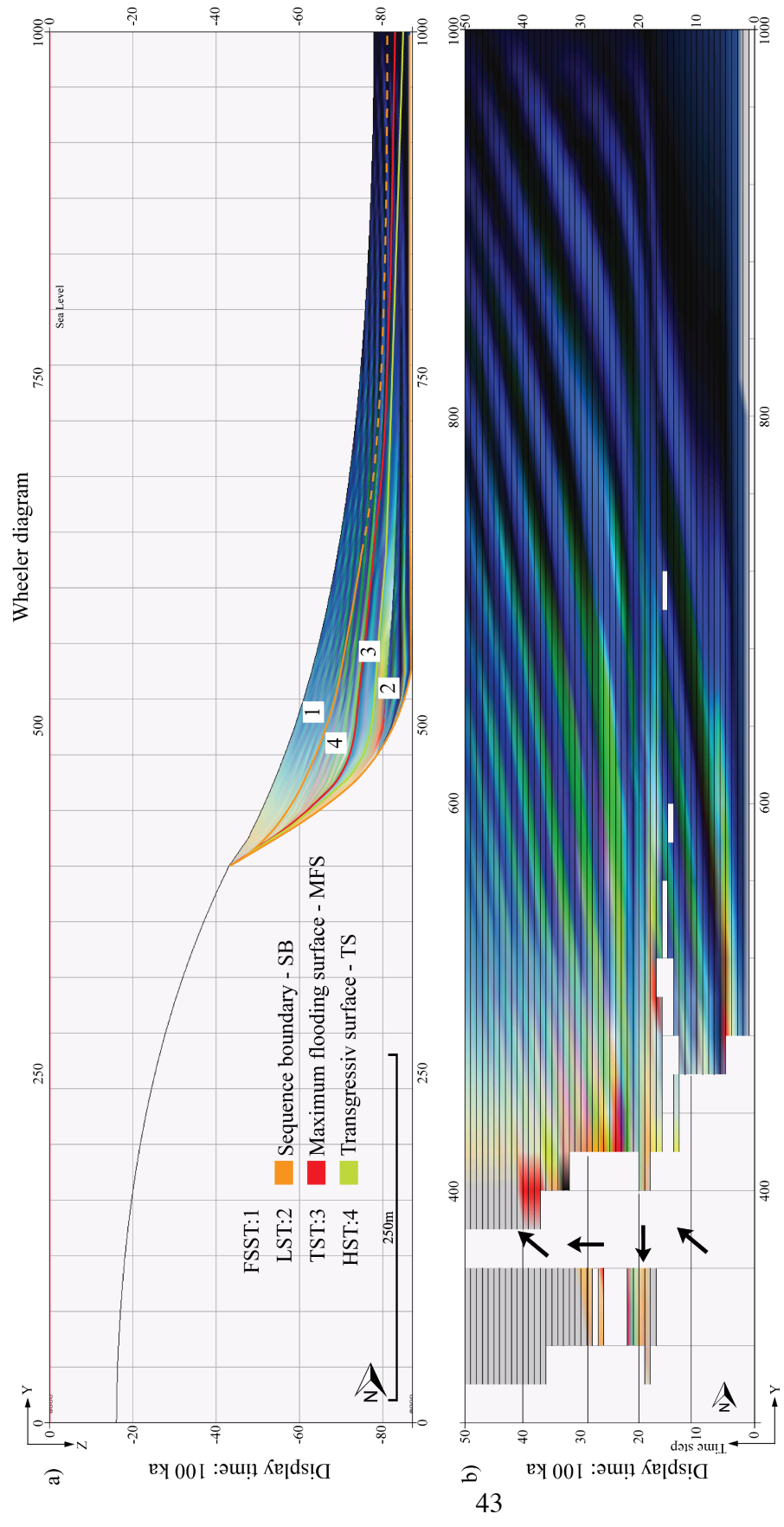


Figure 17: Sinrise model with a larger amplitude of 50 m. The model is 3x vertical exaggerated and displays the final time step at 100 ka. a) Sequence stratigraphy interpretation of N-S cross section. b) N-S Wheeler diagram. Black arrows represent (from bottom to top) aggradation and progradation, retrogradation, aggradation, and progradation.

3.2 Relay ramp

Relay ramps are a type of transfer zones in extensional settings. They consist of two synthetic overlapping normal faults in map view (Morley *et al.*, 1990), where the area between the two normal faults is the relay (Peacock *et al.*, 2000a) (Figure 18). I will consider two models: (i) relay ramp under a slope controlled diffusion process, (ii) relay ramp with a point source and unsteady flow, simulating a turbiditic flow. A larger grid (Figure 19) has been used in both cases, where the total run time for the simulations is 100 ka. The initial surface of the models was tilted (center of rotation $x = 500$ m , $y = 500$ m and $z = 0$) 1° towards NE. The reason for this is to create some initial slope for the second case involving a turbiditic flow. Parameters for the two models are listed in Table 4. Figure 20 shows elevation maps of the relay structure over time, in order to show the tectonic deformation without the interference of other sedimentary processes. During simulation, the development of a long fault structure covering the model from west to east appears. The structure consists of two normal faults, as the tips of these two faults overlap and interact they connect kinematically (Wood, 2013). In response to this, the two faults start to interact laterally and vertically, and the decrease in throw on one fault coincide with the increase in throw on the other fault (Figure 20).

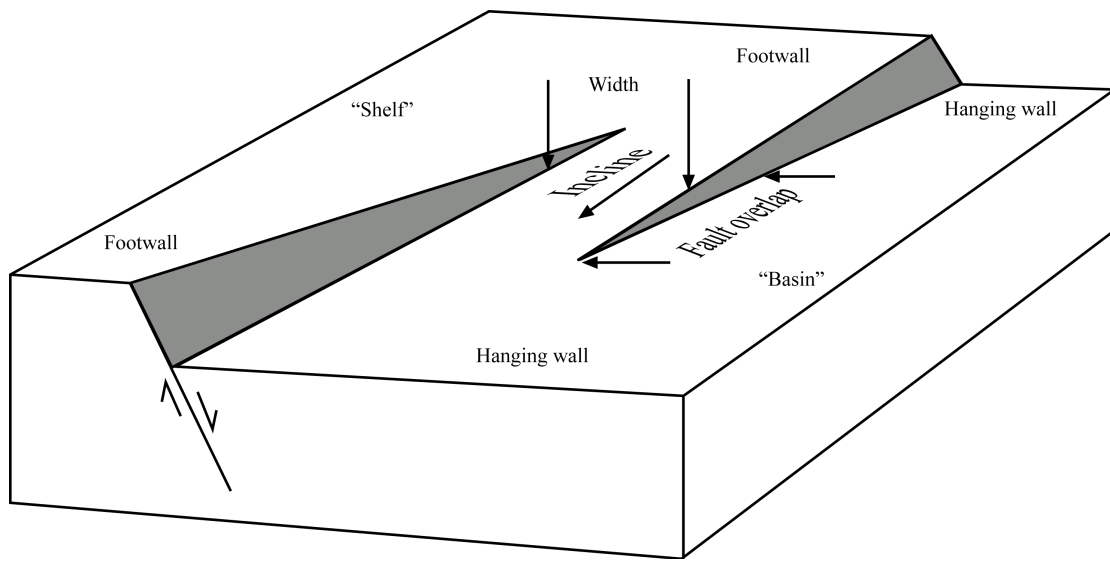


Figure 18: Schematic illustration displaying a relay ramp structure at an early stage, with related terms. (modified after Athmer and Luthi, 2010)

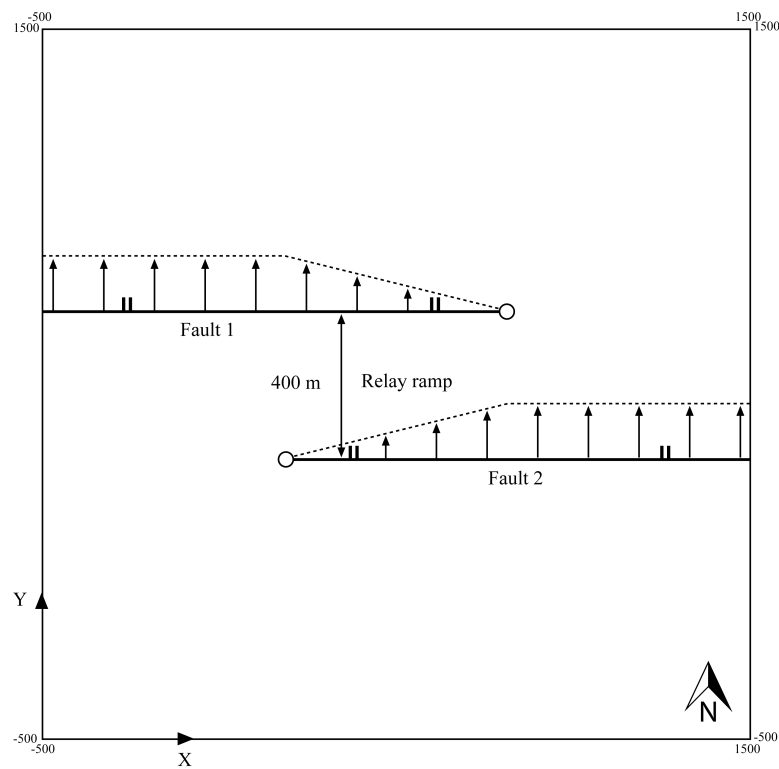


Figure 19: Sketch of the grid with the location of the faults, and the width between the faults. The grid is 2000 m x 2000 m and contains 10 000 cells. Black arrows show the magnitude and sense of fault movement. The faults have constant slip rate on the sides, and the slip rate decreases to zero towards the middle of the model. Note that the faults dip North.

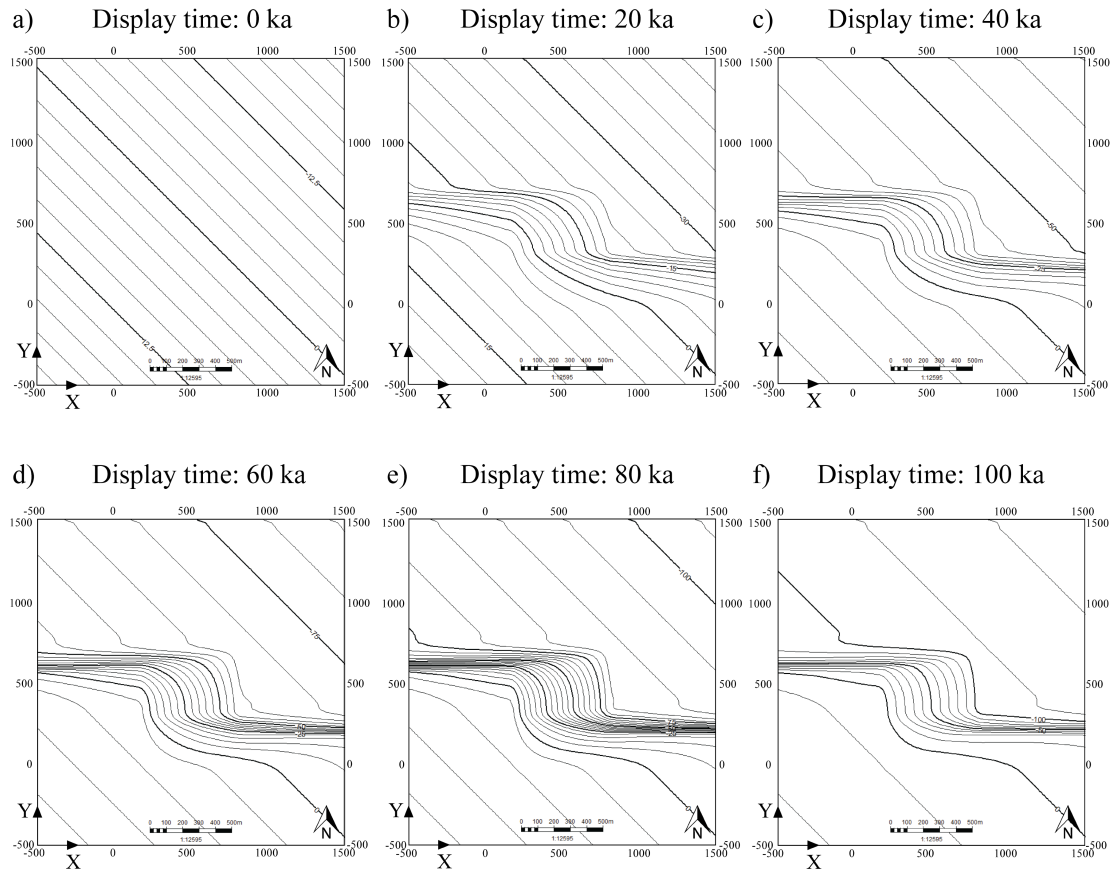


Figure 20: Elevation of relay ramp model over time. a) Model's initial state. b) 20, c) 40, d) 60, e) 80 and f) 100 ka. Only tectonic deformation is shown.

Table 4: List the parameters for the relay ramp simulations, where light grey represent parameters for trishear and dark grey for GPM.

	Relay ramp with diffusion		Relay ramp with unsteady flow	
	Fault 1	Fault 2	Fault 1	Fault 2
Slip rate:	Tip 1: 1 m/ka Tip 2: 0	Tip 1: 0 Tip 2: 1 m/ka	Tip 1: 1 m/ka Tip 2: 0	Tip 1: 0 Tip 2: 1 m/ka
Trishear angle:	60°	60°	60°	60°
P/S:	2	2	2	2
Diffusion rate:	0.07 m ² /a			
Unsteady flow:				
Turbiditic event interval:			4000 a	
Fluid element depth:			1 m	
Duration time:			5 hour	
Display time:			5 hour	
Delta time element:			0.5 sec	
Time factor:			1	
Transport coefficient:			1	

3.2.2 RELAY RAMP WITH DIFFUSION

The first relay ramp model has a diffusion rate of 0.07 m²/a (Table 4). Figure 21 shows a map view, Figure 22 cross sections, and Figure 23 a Wheeler diagram of the model. During simulation, the two synthetic faults propagate upward simultaneously with a fault displacement of 400 m. Early in the simulation (e.g. 10 ka), the influence of trishear deformation is observed, leading to broad folds (e.g. monoclinal) in both sections where the slip rate is constant (e.g. west and east) (Figure 19). The entire structure behaves as one coherent fault, where the amount of displacement and deformation increases over time. Thus, the interaction of the two overlapping fault tips accommodates the displacement, such that the decrease in throw on one fault coincide with the increase in throw on the other fault. The relay ramp is visible at 20 ka (Figure 21b). Between 20 and 40 ka (Figure 21b-c), coarser facies are concentrated near the slope breaks of the two faults. Fine sand (e.g. green) progrades more basinwards in the western section (Wheeler diagram (5), Figure 23), compared to the eastern part (Wheeler diagram (3), Figure 23). At this time interval, the forelimbs of the monoclines steepen as the folds widen (e.g. monocline), due to the propagation of the fault tips and their associated trishear zone. Thus, the sediments are affected by the slope gradient created by trishear, and prograde further down the slope. From 40 to 60 ka (Figure 21c-d), fine sands prograde further into the basin in the western part than in the eastern part (Wheeler diagram (1), Figure 22). Finer facies (e.g. clay silt) gradually start to deposit on top of the fine sand (Figure 21c-d). The faults start to cut the overlying fold, first at the east and west model boundaries (high slip rate) and then gradually towards the central part of the model (low slip rate). The breaching is detected at the slope break, as coarse facies (e.g. red) no longer get deposited (figure 21c-d). Between 60 and 100 ka (Figure 21d-f), breaching of the monocline from both the east and west model boundaries progressively propagates towards the middle of the model along strike. The areas that have been breached become prone to erosion. More erosion occurs in areas where the fault has breached leading to a higher

topography of the areas where the monocline is still growing (e.g. central part of the model). As shown in the Wheeler diagram in Figure 22, coarser facies are deposited in the western section, while finer facies are deposited in the eastern section at the same time. On the N-S cross sections (Figure 23), the thickness of the deposited strata decreases along strike from the eastern (section 3), to the western section (section 5). The ‘mound’ facies pattern displayed in the Wheeler diagram of section 4, which crosses the relay ramp, is a response to the interaction of the two faults.

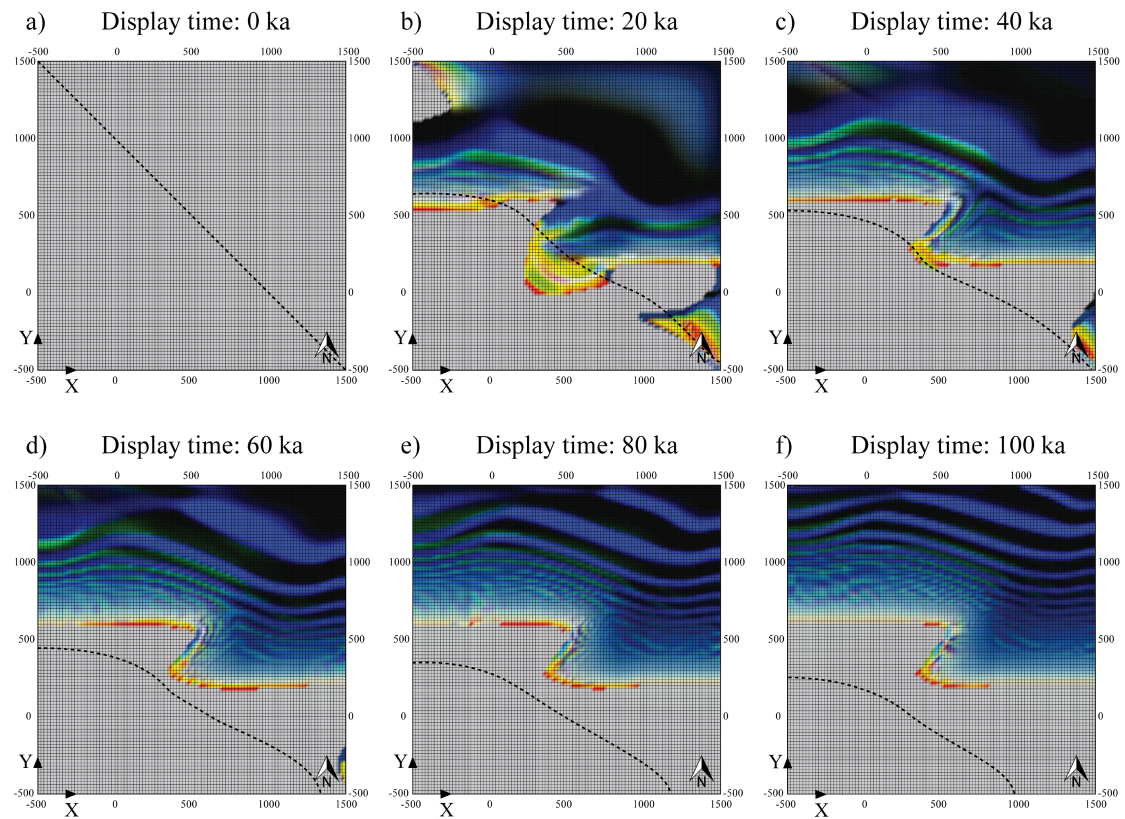


Figure 21: Evolution of relay ramp model with diffusion as map views over time. The black dashed line is the coastline. a) 0, b) 20, c) 40, d) 60, e) 80 and f) 100 ka.

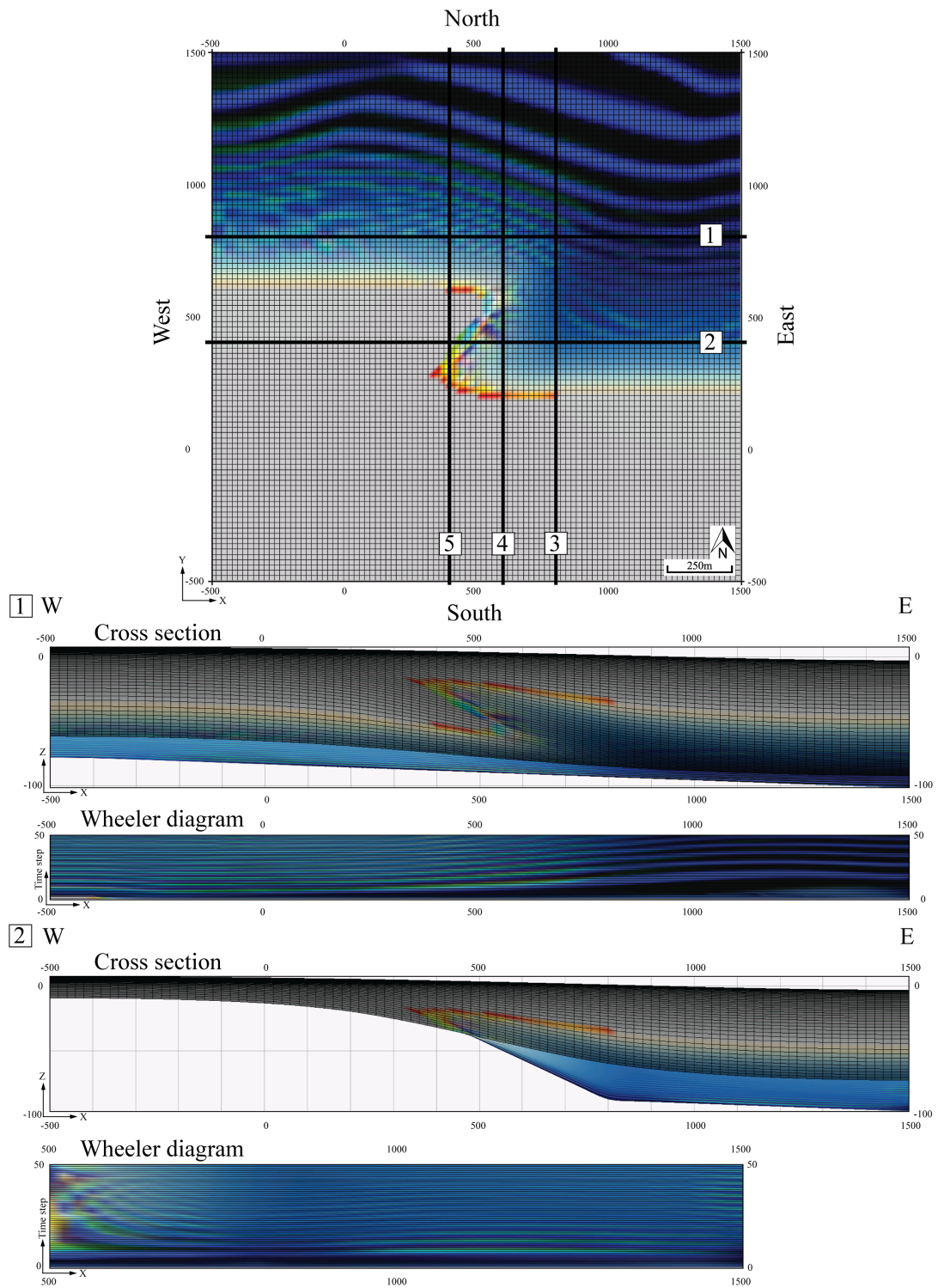


Figure 22: Relay ramp model with diffusion, with corresponding E-W cross sections and Wheeler diagrams (1 and 2). The model is displayed at the final stage 100 ka, the colors represent different facies. Cross sections have 3x vertical exaggeration.

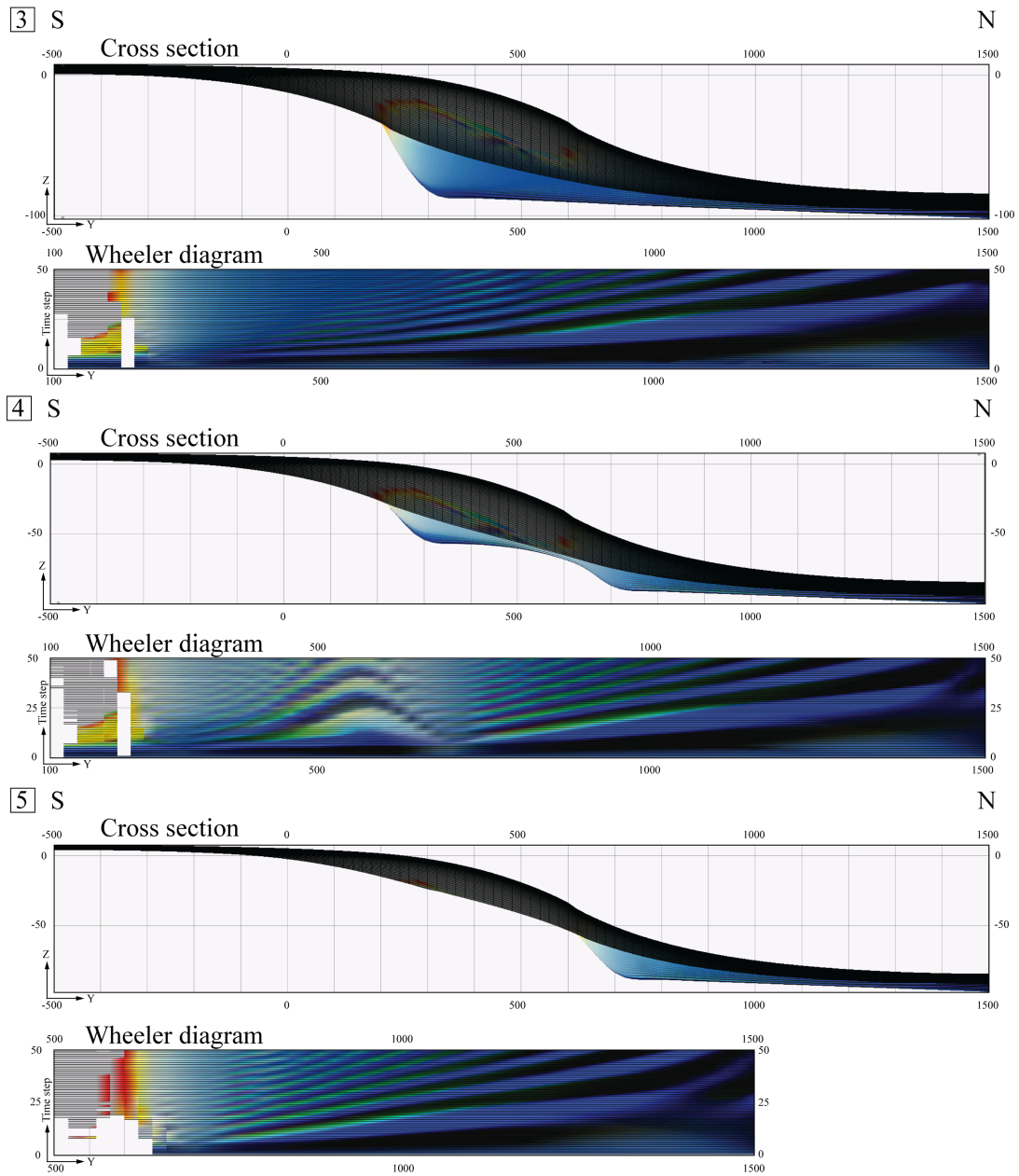


Figure 23: N-S cross sections and Wheeler diagrams of the relay ramp model implemented with diffusion. Location of the sections is on the map view in the previous figure. The model is displayed at the final stage 100 ka, and the colours represent different facies. The cross sections have 3x vertical exaggeration.

3.2.3 RELAY RAMP WITH UNSTEADY FLOW

The aim of this part is to simulate the early evolution of a relay ramp, with a gravity driven sedimentary flow going from the upthrown to the downthrown fault blocks, in the form of a turbiditic flow. I use a point source with a corresponding source map, and unsteady flow for this model. The trishear and GPM parameters in this simulation are included in Table 4. The total run time for the simulation is 100 ka. As mentioned before, the initial surface has a regional NE tilt, thus resulting in an oblique inflow of the unsteady flow. Moreover, the source map including the point source is assumed to be relatively large. This simulates turbidites derived from large deltas near the shoreline and the coastal plain area, under the assumption that these sediments will start to slump downslope, due to a catastrophic event, such a storm or slope failure.

The model is presented first as an elevation map (Figure 24). Between 0 and 20 ka (Figure 24a-b), the turbidite flow finds its way towards the lowest point as expected. As faulting continues throughout the simulation, at 20 ka the faults start to overlap and to interact, and the relay ramp starts to form. Most of the flow (water) at this time ignores the ramp and moves towards the depocenter (NE-corner) crossing the ramp. A small portion of the flow goes perpendicular and deposits sediments at the toe of the slope in the western section. Between 20 and 40 ka, the ramp directs most of the flow and sediments, and lobes start to build up. The erosional flow starts to form channels, which gradually incise deeper over time. From 40 to 60 ka, the forelimbs gradually steepen, and the ramp gets more inclined. The flow starts to erode deeper into the channels, and sediments start to bypass and avulsion (abandonment of channels) occurs. The avulsion is caused by an accumulation of lobes in the end of the ramp, which force the sediments to bypass and deposit in an SW-NE trend. Between 60 and 80 ka, the relay structure has almost reached the final stage. The flow continues to incise, and sediments are deposited on the ramp, resulting in bypass and avulsion, altering the direction of the flow.

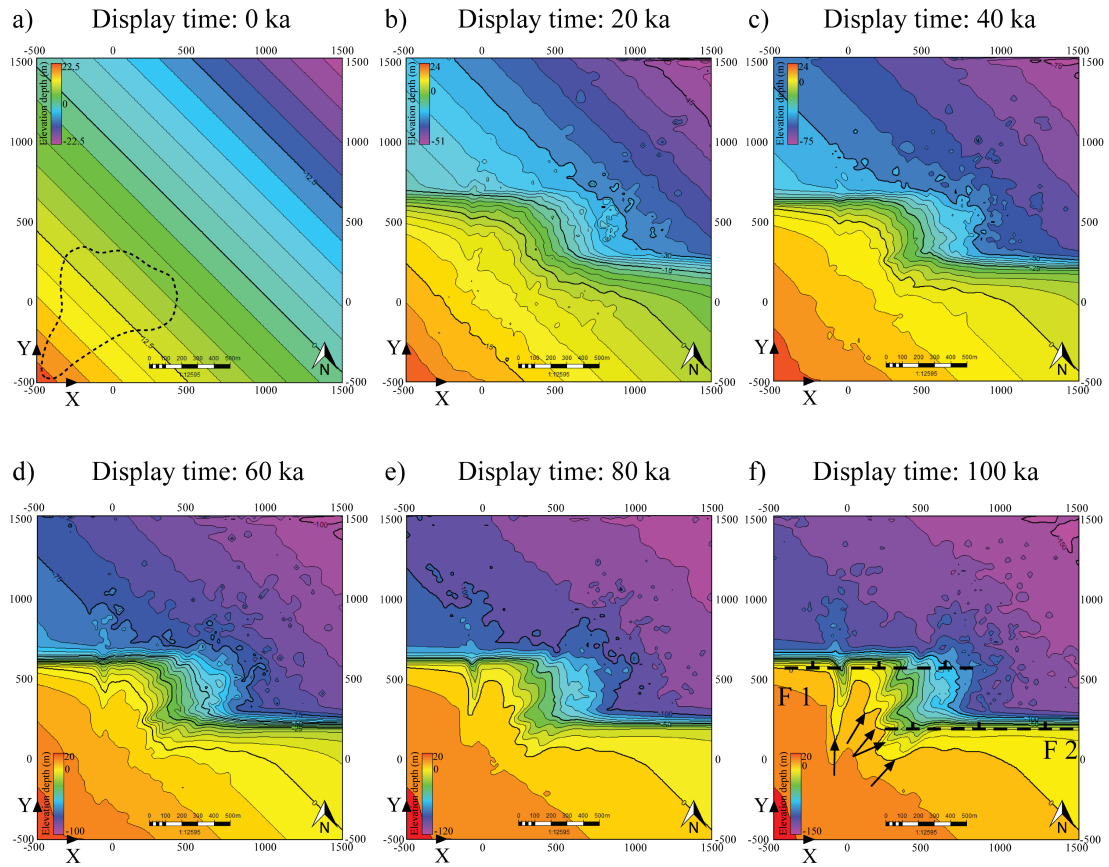


Figure 24: Relay ramp model as elevation maps, where warm colours represent high elevation and cold colours represent low elevation. a) Model's initial state with the outline of the source, b) 20, c) 40, d) 60, e) 80 and f) 100 ka, including faults marking the relay ramp and arrows representing incised channels and direction of flow.

In general, at this late time step, sediments are deposited in a more S–N direction. At the final stage, from 80 to 100 ka, the flow continues to incise deeper into the channels. Parts of the flow not using the ramp as a pathway continue to transport sediments using the incised channels. The parts of the flow directed by the ramp deposit sediments at the toe of the ramp. During the simulation, the model accounts for objects blocking the depositional pathway, which in this model correspond to sedimentary lobes. In response to the blocked pathway, lobes tend to prograde until they avulse (shift) to another part of the fan. The lobes build up on top of the fan surface until the gradient becomes too steep and the flow changes direction to a lower area of the fan, when it no longer can prograde (Nichols, 2009). To get a better insight

into how the lobes are distributed, two figures are presented at the final stage (100 ka) in map view (Figure 25) and six cross-sections (Figure 26). The first E-W section (1, Figure 26) captures the lobes from two locations. The smaller fan is cut in the proximal part of the lobe, and the bigger fan is cut in the central part of the lobe. The second E-W section (2, Figure 26) is more landward, and cuts the lobe complex in the central part, and displays the complex from proximal to distal, from west to east respectively. The third most landward E-W section (3, Figure 26) shows just a small portion of the outer fan. The first N-S section (4, Figure 26) cuts the complex in the outer part of the marginal lobe. The second N-S section (5, Figure 26) exhibits the architecture of the central lobe. The third N-S section (6, Figure 26) displays parts of the lobes deposited on the ramp between $y = 300$ to 600 m. Further north, from $y = 600$ to 1000 m, the section cuts the lobe complex from one of the incised channels.

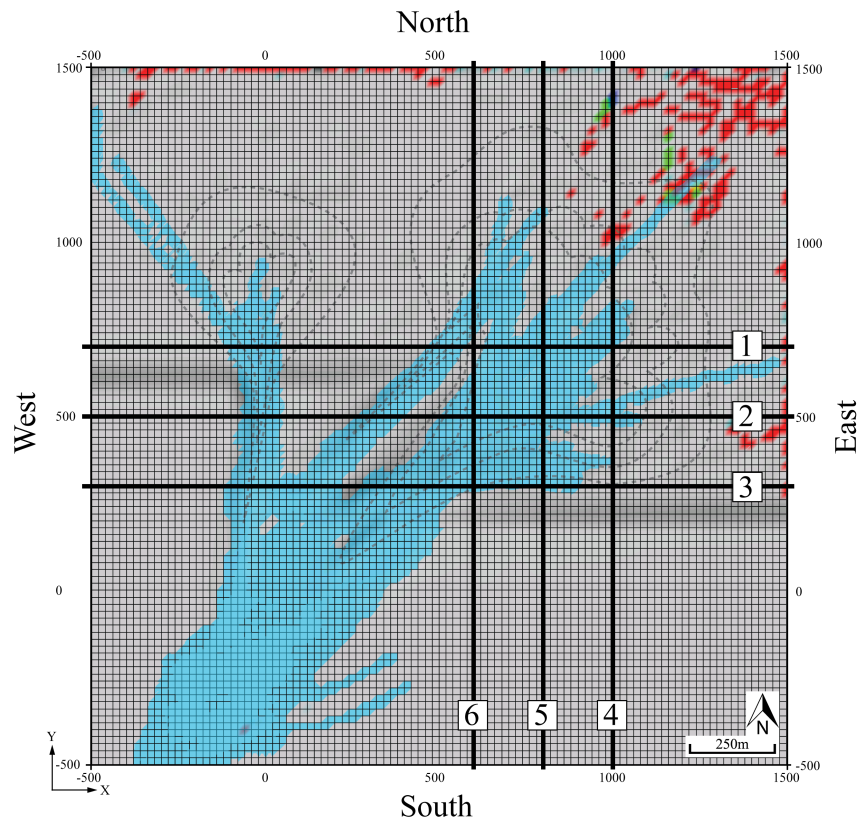


Figure 25: Map view of the relay ramp model with the unsteady flow at 100 ka. Black dashed line is the interpretation of the depositional morphology. Flow is illustrated with blue colours from SW towards NE. Facies are shown in the outer rim of the map. Black lines are the sections in Figure 26.

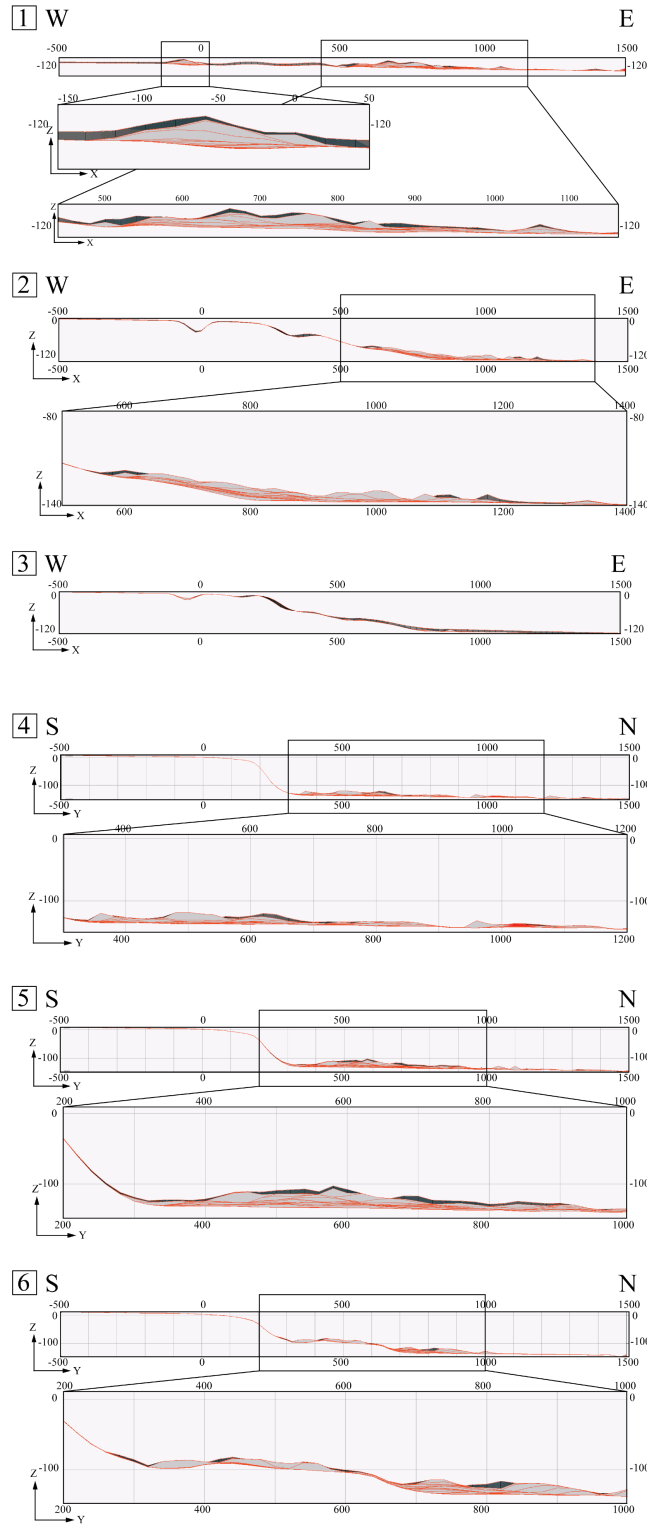


Figure 26: Cross-sections through the relay ramp model with the unsteady flow at 100 ka. Sections 1 - 3 strike E-W, and 4 - 6 N-S. Axes are in meters. Red lines within sedimentary packages represent cycles of 2 ka. Location of sections corresponds with the map in the previous figure. Rectangles on sections show zoomed areas. No vertical exaggeration.

4 DISCUSSION

The main objective of this thesis was to couple the tectonic process of fault-propagation folding with sedimentary processes in the form of erosion, transport, and deposition, in a numerical forward tectono-sedimentary model. This tectono-sedimentary model combines two main tools: trishear fault-propagation folding (Erslev, 1991; Cardozo, 2008) and GPM modelling (Tetzlaff et al., 2014). The implementation consisted in establishing a link between these two tools, such that they could send results to each other during a simulation run. We found Matlab to be a convenient tool for producing trishear results for GPM and reading GPM depositional geometries, but of course, this part can be implemented in another non-commercial platform (e.g. Octave) or language (e.g. Python). Once implemented, the model was applied to two cases: i. A single normal fault is propagating with various trishear parameters along strike, or with constant trishear parameters but various GPM parameters. ii. An extensional relay ramp with an overall slope controlled diffusion process, or with an unsteady flow (e.g. turbidites) process.

The forward model requires the user to specify all initial conditions and input to get a realistic geological result. It is useful to understand the processes that drive and form the sedimentary sequence desired to model. It is key to think geologically and to evaluate the processes (e.g. tectonic and sedimentary) to get the optimum or desired outcome. To reach this understanding, it is important to visualise how tectonics and sedimentation interact with each other. Tectonics acts as a first-order parameter on sedimentation, affecting the topographic relief (e.g. slope) and the sediment source area. Tectonic processes form basins as a result of faulting and determine the 3D geometry and evolution of the basin. Tectonic processes together with sediment and water loading determine the basin subsidence and the accommodation space. Through geological time, tectonics (e.g. rates of seafloor spreading) influences sea level fall

and rise. Changes in sea level together with sediment supply (e.g. controlled by tectonics and climate) and subsidence affect sedimentary processes, depositional environments, sediments properties (e.g., texture, bedding, sedimentary structures), and stratigraphic relationships (e.g., depositional sequences and system tracts) (Boggs, 2001).

This dynamic relationship between tectonics and sedimentary processes is well illustrated in the series of models presented in this thesis. Trishear kinematics together with GPM simulates a physical depositional system where the sedimentary processes interact with the tectonic response in a realistic manner. For example in model VFS (Fig. 10), where variable fault slip rates affect the model to tilt it towards the side with the highest slip rate, the sedimentary processes are influenced such that they result in the deposition of a sedimentary wedge thickening towards the higher fault slip rate regions. Likewise, low trishear angles or P/S result in narrower monoclines and steeper forelimbs, where the diffusion controlled erosional processes are more intense, and coarser facies deposit nearby. Furthermore, the model influenced by eustatic sea level variation (Sinrise), illustrates how significant sea level changes can be on the depositional morphology and sequence stratigraphic framework (Figs. 16-17). The relay ramp model, although tectonically quite simple, illustrate the sedimentary complexity that can be reached when normal faults interact either under diffusion (Figs. 21-23) or unsteady flow (Figs. 24-26).

Being able to visualise the sedimentary bodies in 3D (since GPM is within the Petrel environment), grants the user the opportunity to further explore sections (e.g. perpendicular and along strike, or in time) in greater detail (e.g., facies distribution and thickness). The use of Wheeler diagrams on different directions, also enhance the understanding of the different tectonics and sedimentary processes in space and time. The trishear-GPM implementation and the visualisation environment of GPM (and Petrel) are powerful tools for hydrocarbon exploration, where the primary objective is

to model the physical processes (e.g., tectonic, sedimentary, eustatic) that produced the observed features in subsurface data (e.g. well logs, seismic sections and cores). The workflow described in this thesis is an ideal environment for this purpose: i.e. forward modelling seismic and well data.

The potential for future work is immense. I have just scratched the surface and the potential of the model. From the tectonics point of view, different settings can be introduced (e.g. transfer zones in compressional settings, Higgins et al., 2009), which together with for example unsteady flow (turbiditic currents) can provide an environment for simulating deep water fold and thrust belts. Different tectonic models can also be introduced. An obvious choice will be to derive a simple kinematic model of salt movement, whose contribution on relief depends on the sedimentary loads produced by GPM (e.g. Peel, 2014). From the sedimentary point of view, a reasonable step would be to try more complicated processes such as carbonates deposition. Further refinement of unsteady flow processes (e.g. turbidites) would also be a good way to go. Post-processing of the model results also offers great potential. Since the GPM results are part of a reservoir model, fluid-flow modelling or forward seismic modelling (and seismic sequence stratigraphy) are relatively straightforward. I hope this thesis can contribute to such initiatives.

5 CONCLUSIONS

The presented methodology concerning fault-propagation folding and sedimentary processes illustrate the dynamic relationship between tectonics and sedimentation.

Some general conclusions can be drawn:

- All diffusion-based models display diachronous facies trends younging basinward, with the rate of diachronism proportional to the slope controlled deposition, which in turn is controlled by tectonics.
- Growth-strata geometries combined with tectonic deformation (e.g. extensional fault-propagation folding) are significantly influenced by sea level changes, resulting in distinct system tracts when increasing the amplitude of the eustatic sea level curve.
- When the fault breaches the monocline, the breached area is no longer folded and it is more prone to erosion.
- Synthetic overlapping normal faults that interact produce complex sedimentary bodies.
- Trishear deformation together with GPM models a physical depositional system where the sedimentary processes accommodate the tectonic response in a realistic manner.
- The potential of the derived methodology is significant, either by further elaborating the tectonic or sedimentary models, or by post-processing the model results for fluid flow or seismic response.

6 REFERENCES

- Van Wagoner, J.C., Mitchum, R.M., Capion, K.M., Rahmanian, V.D., 1990. Siliciclastic Sequence Stratigraphy in Well Logs, Cores and Outcrops: Concepts for High-Resolution Correlation of Time and Facies: AAPG Methods in Exploration Series, No.7, pp. 55.
- Allmendinger, R.W., 1998. Inverse and forward numerical modelling of trishear fault-propagation folds: *Tectonics* 17, pp. 640-656.
- Athmer, W., Groenberg, R.M., Luthi, S.M., Donselaar, M.E., Sokoutis, D., Willingshofer, E., 2010. Relay ramps as pathways for turbidity currents: a study combining analogue sandbox experiments and numerical flow simulations: *Sedimentology*, v.57, pp. 806-823.
- Boggs, S., 2001. *Principles of Sedimentology and Stratigraphy*, 3. Edition: Prentice Hall, 726 pp.
- Cardozo, N., 2008. Trishear in 3D. Algorithms, implementation, and limitations: *Journal of Structural Geology*, v.30, pp. 327-340.
- Catuuneau, O., Galloway, W.E., Kendall, C.G.St.C., Miall, A.D., Posamentier, H.W., Strasser, A., & Tucker, M.E., 2011. Sequence Stratigraphy: Method and Nomenclature: *Newsletter on Stratigraphy*, v.44/3, pp. 173-245.
- Cristallini, E.O. & Allmendinger, R.W., 2001. Pseudo 3-D modelling of trishear fault-propagation folding: *Journal of Structural Geology*, v.23, pp. 1883-1899.
- Erslev, E.A., 1991. Trishear fault-propagation folding *Geology*, v.19, pp. 617-620.
- Gawthorpe, R. & Hardy, S., 2002. Extensional fault-propagation folding and base-level change as controls on growth-strata geometries: *Sedimentary Geology*, v.146, pp. 47-56.

- Gawthorpe, R.L., Sharp, I.R., Underhill, J.R., Gupta, S., 1997. Linked sequence stratigraphic and structural evolution of propagating normal faults: *Geology*, v.25, pp. 795-798.
- Grigryev, Y.N., Vashykov V.A., & Fedoruk, M.P., 2002. Numerical Particle-in-cell Methods: Theory and Applications, de Gruyter, 260 pp.
- Hardy, S. & Allmendinger, R.W., 2011. Trishear: A review of kinematics, mechanics, and applications, *In*: McClay, K.R., Shaw, J. & Suppe, J., (Eds.), Thrust fault-related folding: AAPG Memoir 94, pp. 95–119.
- Hardy, S., Ford, M., 1997. Numerical modeling of trishear fault propagation Folding: *Tectonics* v.16, pp. 841-854.
- Higgins, S., Clarke, B., Davies, R.J., Cartwright, L., 2009. Internal geometry and growth history of a thrust-related anticline in a deep water fold belt: *Journal of Structural Geology*, v.31, pp. 1597-1611.
- Morley, C.K., Nelson, R.A., Patton, T.L., Munn, S.G., 1990. Transfer zones in the East African rifts: *Bulletin of the American Association of Petroleum Geologists* v.74, pp. 1234-1253.
- Nichols, G., 2009. *Sedimentology and Stratigraphy*, 2. Edition: Wiley-Blackwell Publication, 419 pp.
- Peacock, D.C.P., Knipe, R.J., Sanderson, D.J., 2000. Glossary of normal faults: *Journal of Structural Geology* v.22, pp. 291-305.
- Peel, F.J., 2014. How do salt withdrawal minibasins form? Insights from forward modelling, and implications for hydrocarbon migration: *Tectonophysics*, v.630, pp. 222-235.
- Petrel *2015.4 Sedimentary Simulation and Visualization Plug-in Version: 1.0.6.0 (Nov70172016) Schlumberger

- Tetzlaff, D., Tveiten, J., Salomonsen, P., Christ, A., Athmer, W., Borgos, B.G., Sonneland, L., Claudia, M. & Raggio, M.F., 2014. Geologic Process Modeling: IX Congreso de Exploración y Desarrollo de Hidrocarburos - IAPG, Mendoza City, Argentina, pp. 1-16.
- Van Wagoner, J.C., Posamentier, H.W., Mitchum, R.M., Vail, P.R., Sarg, J.F., Loutit, T.S., & Hardenbol, L., 1988. An overview of sequence stratigraphy and key definitions, *In*: Wilgus, C.W., et al., (Eds.), Sea level changes: an integrated approach: Society of Economic Paleontologist and Mineralogist Special Publication 42, pp. 39-45.
- Wheeler, H.E., 1964. Baselevel, Lithosphere Surface, and Time-Stratigraphy: Geological Society of America Bulletin, v.75, pp. 599-610.
- Wood, A.M., 2013. The influence of fault geometric uncertainty on hydrocarbon reservoir and simulation models. Ph.D. Doctoral thesis, University of Leeds. Retrieved
- Zehender, A.T., Allmendinger, R.W., 2000. Velocity field for the trishear model: Journal of Structural Geology v.22, pp. 1009-1014.

APPENDIX: TRISHEAR SCRIPTS BY NESTOR CARDOZO

trishear.m (single normal fault)

```
% trishear: Pseudo 3D trishear: One single normal fault
% trishear uses script gridfit by John D'Errico (2006)
% Author: Nestor Cardozo, email: nestor.cardozo@uis.no

%-----
% THESE PARAMETERS CAN BE MODIFIED BY THE USER
%-----

strike = 270.0*pi/180.0; % strike of fault
ramp = 60.0*pi/180.0; % dip of fault
%
% Current tips should be saved in a .mat file, see included .mat file
load tips.mat; % fault tips (1 = xts, yts, zts; 2 = xtn, ytn, ztn)
%
pss = 1.5; % propagation to slip ratio at fault tip 1
psn = 1.5; % propagation to slip ratio at fault tip 2
tras = 60.0*pi/180; % trishear angle at fault tip 1
tran = 60.0*pi/180; % trishear angle at fault tip 2
slrs = -1e-3; % slip rate tip 1 (1 m/ka), negative is for normal fault
slrn = -1e-3; % slip rate tip 2 (1 m/ka), negative is for normal fault
timestep = 1e3; % timestep from GMP in years
sls = slrs*timestep; % slip tip 1 (in m)
sln = slrn*timestep; % slip tip 2 (in m)
ninc = 10; % Since the amount of slip is small, we don't need many intervals
slrake = 90*pi/180; % slip rake
%-----

% Load file from GMP
filename = 'input.csv'; % filename from GMP
delimiterIn = ','; % comma delimiter
headerlinesIn = 1; % single column header
A = importdata(filename,delimiterIn,headerlinesIn);

% make grid
nz = max(A.data(:,1)); % number of layers assuming layer index is in first column
ny = max(A.data(:,2)); % number of rows
```

```

nx = max(A.data(:,3)); %number of columns
XP = zeros(ny,nx,nz);
YP = zeros(ny,nx,nz);
ZP = zeros(ny,nx,nz);

% read nodes from GMP, assuming nodes change first in x, then y, then z
count = 1;
for i=1:nz % varies third in z
    for j=1:ny % varies second in y
        for k=1:nx % varies first in x
            XP(j,k,i) = A.data(count,4);
            YP(j,k,i) = A.data(count,5);
            ZP(j,k,i) = A.data(count,6);
            count = count + 1;
        end
    end
end

% For interpolation to GPM grid
xpi = XP(1,:,1);
ypi = YP(:,1,1)';
XPI=XP; % x of GPM nodes
YPI=YP; % y of GPM nodes
ZPI = zeros(ny,nx,nz);

% Pseudo 3D trishear

%-----
% Coordinate systems

% The first coordinate system is the XP (east), YP(north), ZP(up) system,
% which is used for plotting. The direction cosines of this system (North, East, Down)
% are:

% For XP (east) axis
dcosxp2=1.0; %dcosxp1, and dcosxp3 are zero
% For YP (north) axis
dcosyp1=1.0; %dcosyp2, and dcosyp3 are zero
% For ZP (up) axis
dcoszp3=-1.0; %dcoszp1, and dcoszp2 are zero

% The slip vector trend and plunge are
striked = strike*180.0/pi;

```



```

if (slrake <= pi/2.)
    slrakef = slrake;
else
    slrakef = pi-slrake;
end
angle1 = atan(tan(slrakef)*cos(ramp))*180.0/pi;
if (slrake <= pi/2.)
    oppstriked = striked + 180.0;
    if (oppstriked >= 360.0)
        oppstriked = oppstriked - 360.0;
    end
    sltrend = oppstriked + angle1;
    if (sltrend >= 360.0)
        sltrend = sltrend - 360.0;
    end
else
    sltrend = striked - angle1;
    if (sltrend < 0.0)
        sltrend = sltrend + 360.0;
    end
end
end
sltrend = sltrend*pi/180.0;
slplunge=asin(sin(slrakef)*sin(ramp));

% The second coordinate system is the FX (parallel to fault slip),
% FY (perpendicular to fault plane) and FZ (perpendicular to fault
% slip) system. The FX, FY, FZ system has the following direction
% cosines (North, east, down):

% For the FX (parallel to fault slip) axis
dcosfx1=cos(sltrend)*cos(slplunge);
dcosfx2=sin(sltrend)*cos(slplunge);
dcosfx3=-sin(slplunge);

% For the FY (perpendicular to fault plane) axis
angle1 = striked + 90.0;
if (angle1 >= 360.0)
    angle1 = angle1 - 360.0;
end
angle1 = angle1*pi/180.0;
dcosfy1=cos(angle1)*cos(pi/2.0-ramp);
dcosfy2=sin(angle1)*cos(pi/2.0-ramp);

```

```

dcosfy3=-sin(pi/2.0-ramp);

% For the FZ (perpendicular to fault slip) axis, use the cross product
% between FX and FY
dcosfz1=dcosfx2*dcosfy3-dcosfx3*dcosfy2;
dcosfz2=dcosfx3*dcosfy1-dcosfx1*dcosfy3;
dcosfz3=dcosfx1*dcosfy2-dcosfx2*dcosfy1;

% The transformation matrix between the XP-YP-ZP system and the FX-FY-FZ system
% is therefore:
% cosine of the angle between FX and XP
gp11=dcosfx2*dcosxp2;
% cosine of the angle between FX and YP
gp12=dcosfx1*dcosyp1;
% cosine of the angle between FX and ZP
gp13=dcosfx3*dcoszp3;
% cosine of the angle between FY and XP
gp21=dcosfy2*dcosxp2;
% cosine of the angle between FY and YP
gp22=dcosfy1*dcosyp1;
% cosine of the angle between FY and ZP
gp23=dcosfy3*dcoszp3;
% cosine of the angle between FZ and XP
gp31=dcosfz2*dcosxp2;
% cosine of the angle between FZ and YP
gp32=dcosfz1*dcosyp1;
% cosine of the angle between FZ and ZP
gp33=dcosfz3*dcoszp3;

% BEDS, TRANSFORM XP,YP, ZP TO FX,FY,FZ COORDINATE SYSTEM
% WITH ORIGIN AT THE SOUTHERN FAULT TIP
FX= (XP-xts)*gp11+(YP-yts)*gp12+(ZP-zts)*gp13;
FY= (XP-xts)*gp21+(YP-yts)*gp22+(ZP-zts)*gp23;
FZ= (XP-xts)*gp31+(YP-yts)*gp32+(ZP-zts)*gp33;

% transform northern tip to FX, FY, FZ coordinate system
% WITH ORIGIN AT THE SOUTHERN FAULT TIP
northtipfx = (xtn-xts)*gp11+(ytn-yts)*gp12+(ztn-zts)*gp13;
northtipfz = (xtn-xts)*gp31+(ytn-yts)*gp32+(ztn-zts)*gp33;

%-----

```

```

% Variation of trishear parameters along T1
T1 = northtipfz;
% Variation of P/S
Aps = (psn-pss)/T1;
% Half trishear angle and variation
htran = tran/2.0;
htras = tras/2.0;
Ata = (htran-htras)/T1;
% incremental slip and variation
sincs = sls/ninc;
sincn = sln/ninc;
Av = (sincn-sincs)/T1;

%-----
% RUN TRISHEAR
for i=1:ninc
    for j=1:size(FX,1)
        for k=1:size(FX,2)
            for l=1:size(FX,3)
                % P/S
                ps = Aps*FZ(j,k,l)+pss;
                % half trishear angle
                htra = Ata*FZ(j,k,l)+htras;
                m = tan(htra);
                % slip increment
                sinc = Av*FZ(j,k,l)+sincs;
                % Notice that in the case of a slip vector not
                % perpendicular to the tip line, I have to correct
                % for the distance between XP = 0 and the tip line
                % I do this by subtracting (FZ(j,k,l)/northtipfz)*northtipfx to xx
                % NOTE: MOVE TIP FORWARD AND THEN DEFORM
                xx=FX(j,k,l)- (FZ(j,k,l)/northtipfz)*northtipfx - ps*i*(abs(sinc));
                yy=FY(j,k,l);
                [vx,vy]=veltrishear(xx,yy,sinc,m);
                % update FX, FY coordinates
                FX(j,k,l)= FX(j,k,l) + vx;
                FY(j,k,l) = FY(j,k,l) + vy;
            end
        end
    end
end
end
end

```

```

%-----

% TRANSFORM FX-FY-FZ TO XP-YP-ZP COORDINATE SYSTEM
XP= FX*gp11+FY*gp21+FZ*gp31+xts;
YP= FX*gp12+FY*gp22+FZ*gp32+yts;
ZP= FX*gp13+FY*gp23+FZ*gp33+zts;

% INTERPOLATE to GPM grid: Use script gridfit by John D'Errico
for i=1:nz
    ZPI(:, :, i) = gridfit(XP(:, :, i), YP(:, :, i), ZP(:, :, i), xpi, ypi, 'extend', 'always');
end

% write file to GPM
fid = fopen('out.csv', 'wt');
fprintf(fid, 'Layer (index), I (index), J (index), X, Y, Z\n');
for i=1:nz % varies second in z
    for j=1:ny % varies second in y
        for k=1:nx % varies first in x
            fprintf(fid, '%i, %i, %i, %f, %f, %f\n', i, j, k, XPI(j, k, i), YPI(j, k, i), ZPI(j, k, i));
        end
    end
end
fclose(fid);

% Fault tips
xts = xts+pss*abs(sls)*gp11;
xtn = xtn+psn*abs(sln)*gp11;
yts = yts+pss*abs(sls)*gp12;
ytn = ytn+psn*abs(sln)*gp12;
zts = zts+pss*abs(sls)*gp13;
ztn = ztn+psn*abs(sln)*gp13;

% Write tips to tips.mat file
save tips.mat xts yts zts xtn ytn ztn;

% exit matlab
exit;

```

trishear.m (relay ramp)

```
% trishear: Pseudo 3D trishear: Relay ramp case
% trishear uses script gridfit by John D'Errico (2006)
% Author: Nestor Cardozo, email: nestor.cardozo@uis.no

%-----
% THESE PARAMETERS CAN BE MODIFIED BY THE USER
%-----

strike = 270.0*pi/180.0; % strike of faults 1 and 2
ramp = 60.0*pi/180.0; % dip of faults 1 and 2
%
% Current tips should be saved in a .mat file, see included .mat file
% fault 1 tips (1 = xt1s, yt1s, zt1s; 2 = xt1n, yt1n, zt1n)
% fault 2 tips (1 = xt2s, yt2s, zt2s; 2 = xt2n, yt2n, zt2n)
load tips.mat;
% p/s, trishear angle and slip for fault 1
pss1 = 2.; % propagation to slip ratio at fault tip 1
psn1 = 2.; % propagation to slip ratio at fault tip 2
tras1 = 60.0*pi/180; % trishear angle at fault tip 1
tran1 = 60.0*pi/180; % trishear angle at fault tip 2
slrs1 = -1e-3; % slip rate tip 1 in m, negative is for normal fault
slrn1 = 0; % slip rate tip 2 in m, negative is for normal fault
%
% p/s, trishear angle and slip for fault 2
pss2 = 2.; % propagation to slip ratio at fault tip 1
psn2 = 2.; % propagation to slip ratio at fault tip 2
tras2 = 60.0*pi/180; % trishear angle at fault tip 1
tran2 = 60.0*pi/180; % trishear angle at fault tip 2
slrs2 = 0; % slip rate tip 1 in m, negative is for normal fault
slrn2 = -1e-3; % slip rate tip 2 in m, negative is for normal fault
%
timestep = 2e3; % timestep or display increment in GMP in years
%
sls1 = slrs1*timestep; % slip fault 1 tip 1 (in m)
sln1 = slrn1*timestep; % slip fault 1 tip 2 (in m)
sls2 = slrs2*timestep; % slip fault 2 tip 1 (in m)
sln2 = slrn2*timestep; % slip fault 2 tip 2 (in m)
%
```

```

slrake = 90*pi/180; % slip rake
ninc = 10; % Since the amount of slip is small, we don't need many intervals
%-----

% Load file from GMP
filename = 'input.csv'; % filename from GMP
delimiterIn = ','; % comma delimiter
headerlinesIn = 1; % single column header
A = importdata(filename,delimiterIn,headerlinesIn);

% make grid
nz = max(A.data(:,1)); % number of layers assuming layer index is in first column
ny = max(A.data(:,2)); %number of rows
nx = max(A.data(:,3)); %number of columns
XP = zeros(ny,nx,nz);
YP = zeros(ny,nx,nz);
ZP = zeros(ny,nx,nz);

% read nodes from GMP, assuming nodes change first in x, then y, then z
count = 1;
for i=1:nz % varies third in z
    for j=1:ny % varies second in y
        for k=1:nx % varies first in x
            XP(j,k,i) = A.data(count,4);
            YP(j,k,i) = A.data(count,5);
            ZP(j,k,i) = A.data(count,6);
            count = count + 1;
        end
    end
end

% For interpolation to GPM grid
xpi = XP(1,:,1);
ypi = YP(:,1,1)';
XPI=XP; % x of GPM nodes
YPI=YP; % y of GPM nodes
ZPI = zeros(ny,nx,nz);

% Pseudo 3D trishear
%-----

% Coordinate systems

```

```

% The first coordinate system is the XP (east), YP(north), ZP(up) system,
% which is used for plotting. The direction cosines of this system (North, East, Down)
% are:

% For XP (east) axis
dcosxp2=1.0; %dcosxp1, and dcosxp3 are zero
% For YP (north) axis
dcosyp1=1.0; %dcosyp2, and dcosyp3 are zero
% For ZP (up) axis
dcoszp3=-1.0; %dcoszp1, and dcoszp2 are zero

%-----
% The slip vector trend and plunge are
striked = strike*180.0/pi;
if (slrake <= pi/2.)
    slrakef = slrake;
else
    slrakef = pi-slrake;
end
angle1 = atan(tan(slrakef)*cos(ramp))*180.0/pi;
if (slrake <= pi/2.)
    oppstriked = striked + 180.0;
    if (oppstriked >= 360.0)
        oppstriked = oppstriked - 360.0;
    end
    sltrend = oppstriked + angle1;
    if (sltrend >= 360.0)
        sltrend = sltrend - 360.0;
    end
else
    sltrend = striked - angle1;
    if (sltrend < 0.0)
        sltrend = sltrend + 360.0;
    end
end
sltrend = sltrend*pi/180.0;
slplunge=asin(sin(slrakef)*sin(ramp));
% The second coordinate system is the FX (parallel to fault slip),
% FY (perpendicular to fault plane) and FZ (perpendicular to fault
% slip) system. The FX, FY, FZ system has the following direction
% cosines (North, east, down):
% For the FX (parallel to fault slip) axis
dcosfx1=cos(sltrend)*cos(slplunge);

```

```

dcosfx2=sin(sltrend)*cos(slplunge);
dcosfx3=-sin(slplunge);
% For the FY (perpendicular to fault plane) axis
angle1 = striked + 90.0;
if (angle1 >= 360.0)
    angle1 = angle1 - 360.0;
end
angle1 = angle1*pi/180.0;
dcosfy1=cos(angle1)*cos(pi/2.0-ramp);
dcosfy2=sin(angle1)*cos(pi/2.0-ramp);
dcosfy3=-sin(pi/2.0-ramp);
% For the FZ (perpendicular to fault slip) axis, use the cross product
% between FX and FY
dcosfz1=dcosfx2*dcosfy3-dcosfx3*dcosfy2;
dcosfz2=dcosfx3*dcosfy1-dcosfx1*dcosfy3;
dcosfz3=dcosfx1*dcosfy2-dcosfx2*dcosfy1;
% The transformation matrix between the XP-YP-ZP system and the FX-FY-FZ system
% is therefore:
% cosine of the angle between FX and XP
gp11=dcosfx2*dcosxp2;
% cosine of the angle between FX and YP
gp12=dcosfx1*dcosyp1;
% cosine of the angle between FX and ZP
gp13=dcosfx3*dcoszp3;
% cosine of the angle between FY and XP
gp21=dcosfy2*dcosxp2;
% cosine of the angle between FY and YP
gp22=dcosfy1*dcosyp1;
% cosine of the angle between FY and ZP
gp23=dcosfy3*dcoszp3;
% cosine of the angle between FZ and XP
gp31=dcosfz2*dcosxp2;
% cosine of the angle between FZ and YP
gp32=dcosfz1*dcosyp1;
% cosine of the angle between FZ and ZP
gp33=dcosfz3*dcoszp3;
%-----
% Fault 1
% transform northern tip to FX, FY, FZ coordinate system
% WITH ORIGIN AT THE SOUTHERN FAULT TIP
northtipfx1 = (xt1n-xt1s)*gp11+(yt1n-yt1s)*gp12+(zt1n-zt1s)*gp13;
northtipfz1 = (xt1n-xt1s)*gp31+(yt1n-yt1s)*gp32+(zt1n-zt1s)*gp33;

```



```

%-----
% Variation of trishear parameters along T1
T1 = northtipfz1;
% Variation of P/S
Aps1 = (psn1-pss1)/T1;
% Half trishear angle and variation
htran1 = tran1/2.0;
htras1 = tras1/2.0;
Ata1 = (htran1-htras1)/T1;
% incremental slip and variation
sincs1 = sls1/ninc;
sincn1 = sln1/ninc;
Av1 = (sincn1-sincs1)/T1;

%-----
% Fault 2
% transform northern tip to FX, FY, FZ coordinate system
% WITH ORIGIN AT THE SOUTHERN FAULT TIP
northtipfx2 = (xt2n-xt2s)*gp11+(yt2n-yt2s)*gp12+(zt2n-zt2s)*gp13;
northtipfz2 = (xt2n-xt2s)*gp31+(yt2n-yt2s)*gp32+(zt2n-zt2s)*gp33;
%-----
% Variation of trishear parameters along T21
T2 = northtipfz2;
% Variation of P/S
Aps2 = (psn2-pss2)/T2;
% Half trishear angle and variation
htran2 = tran2/2.0;
htras2 = tras2/2.0;
Ata2 = (htran2-htras2)/T2;
% incremental slip and variation
sincs2 = sls2/ninc;
sincn2 = sln2/ninc;
Av2 = (sincn2-sincs2)/T2;
%-----

% RUN TRISHEAR
for i=1:ninc
    %-----
    % Fault 1
    % BEDS, TRANSFORM XP,YP, ZP TO FX,FY,FZ COORDINATE SYSTEM
    % WITH ORIGIN AT THE SOUTHERN FAULT TIP
    FX= (XP-xt1s)*gp11+(YP-yt1s)*gp12+(ZP-zt1s)*gp13;

```

```

FY= (XP-xtls)*gp21+(YP-ytls)*gp22+(ZP-ztls)*gp23;
FZ= (XP-xtls)*gp31+(YP-ytls)*gp32+(ZP-ztls)*gp33;
for j=1:size(FX,1)
    for k=1:size(FX,2)
        for l=1:size(FX,3)
            % P/S
            ps = Aps1*FZ(j,k,l)+pss1;
            % half trishear angle
            htra = Atal*FZ(j,k,l)+htras1;
            m = tan(htra);
            % slip increment
            sinc = Av1*FZ(j,k,l)+sincs1;
            % avoid positive/reverse slip
            if sinc > 0.0
                sinc = 0.0;
            end
            % avoid slip larger than maximum specified slip on fault tip
            if sinc < sincs1
                sinc = sincs1;
            end
            % Notice that in the case of a slip vector not
            % perpendicular to the tip line, I have to correct
            % for the distance between XP = 0 and the tip line
            % I do this by subtracting (FZ(j,k,l)/northtipfz)*northtipfx to xx
            % NOTE: MOVE TIP FORWARD AND THEN DEFORM
            xx=FX(j,k,l)- (FZ(j,k,l)/northtipfz1)*northtipfx1 - ps*i*(abs(sinc));
            yy=FY(j,k,l);
            [vx,vy]=veltrishear(xx,yy,sinc,m);
            % update FX, FY coordinates
            FX(j,k,l)= FX(j,k,l) + vx;
            FY(j,k,l) = FY(j,k,l) + vy;
        end
    end
end
% TRANSFORM FX-FY-FZ TO XP-YP-ZP COORDINATE SYSTEM
XP= FX*gp11+FY*gp21+FZ*gp31+xtls;
YP= FX*gp12+FY*gp22+FZ*gp32+ytls;
ZP= FX*gp13+FY*gp23+FZ*gp33+ztls;
%-----

%-----

% Fault 2

```

```

% BEDS, TRANSFORM XP,YP, ZP TO FX,FY,FZ COORDINATE SYSTEM
% WITH ORIGIN AT THE SOUTHERN FAULT TIP
FX= (XP-xt2s)*gp11+(YP-yt2s)*gp12+(ZP-zt2s)*gp13;
FY= (XP-xt2s)*gp21+(YP-yt2s)*gp22+(ZP-zt2s)*gp23;
FZ= (XP-xt2s)*gp31+(YP-yt2s)*gp32+(ZP-zt2s)*gp33;
for j=1:size(FX,1)
    for k=1:size(FX,2)
        for l=1:size(FX,3)
            % P/S
            ps = Aps2*FZ(j,k,l)+pss2;
            % half trishear angle
            htra = Ata2*FZ(j,k,l)+htras2;
            m = tan(htra);
            % slip increment, avoid interpolating beyond the fault tip
            sinc = Av2*FZ(j,k,l)+sincs2;
            % avoid positive/reverse slip
            if sinc > 0.0
                sinc = 0.0;
            end
            % avoid slip larger than maximum specified slip on fault tip
            if sinc < sincn2
                sinc = sincn2;
            end
            % Notice that in the case of a slip vector not
            % perpendicular to the tip line, I have to correct
            % for the distance between XP = 0 and the tip line
            % I do this by subtracting (FZ(j,k,l)/northtipfz)*northtipfx to xx
            % NOTE: MOVE TIP FORWARD AND THEN DEFORM
            xx=FX(j,k,l)- (FZ(j,k,l)/northtipfz2)*northtipfx2 - ps*i*(abs(sinc));
            yy=FY(j,k,l);
            [vx,vy]=veltrishear(xx,yy,sinc,m);
            % update FX, FY coordinates
            FX(j,k,l)= FX(j,k,l) + vx;
            FY(j,k,l) = FY(j,k,l) + vy;
        end
    end
end
% TRANSFORM FX-FY-FZ TO XP-YP-ZP COORDINATE SYSTEM
XP= FX*gp11+FY*gp21+FZ*gp31+xt2s;
YP= FX*gp12+FY*gp22+FZ*gp32+yt2s;
ZP= FX*gp13+FY*gp23+FZ*gp33+zt2s;
%-----

```

```

end

%-----

%Update fault tips
% Fault 1 final
xt1s = xt1s+pss1*abs(sls1)*gpl1;
xt1n = xt1n+psn1*abs(sln1)*gpl1;
yt1s = yt1s+pss1*abs(sls1)*gpl2;
yt1n = yt1n+psn1*abs(sln1)*gpl2;
zt1s = zt1s+pss1*abs(sls1)*gpl3;
zt1n = zt1n+psn1*abs(sln1)*gpl3;
% Fault 2 final
xt2s = xt2s+pss2*abs(sls2)*gpl1;
xt2n = xt2n+psn2*abs(sln2)*gpl1;
yt2s = yt2s+pss2*abs(sls2)*gpl2;
yt2n = yt2n+psn2*abs(sln2)*gpl2;
zt2s = zt2s+pss2*abs(sls2)*gpl3;
zt2n = zt2n+psn2*abs(sln2)*gpl3;

% INTERPOLATE to GPM grid: Use script gridfit by John D'Errico
for i=1:nz
    ZPI(:, :, i) = gridfit(XP(:, :, i), YP(:, :, i), ZP(:, :, i), xpi, ypi, 'extend', 'always');
end

% write file to GPM
fid = fopen('out.csv', 'wt');
fprintf(fid, 'Layer (index), I (index), J (index), X, Y, Z\n');
for i=1:nz % varies second in z
    for j=1:ny % varies second in y
        for k=1:nx % varies first in x
            fprintf(fid, '%i, %i, %i, %f, %f, %f\n', i, j, k, XPI(j, k, i), YPI(j, k, i), ZPI(j, k, i));
        end
    end
end
end
fclose(fid);

% Write tips to tips.mat file
save tips.mat xt1s yt1s zt1s xt1n yt1n zt1n xt2s yt2s zt2s xt2n yt2n zt2n;

% exit matlab

```

```
exit;
```

veltrishear.m (simplest velocity of trishear model)

```
% Trishear velocity field
% Author: Nestor Cardozo, nestor.cardozo@uis.no

function [vx, vy] = veltrishear(xx,yy,sinc,m)

% 2D
% simplest velocity of trishear model
% algorithm from Zehnder and Allmendinger (2000)

if xx < 0.0
    if yy >= 0.0
        vx = sinc;
        vy = 0.0;
    elseif yy < 0.0
        vx = 0.0;
        vy = 0.0;
    end
elseif xx >= 0.0
    if yy >= xx*m
        vx = sinc;
        vy = 0.0;
    elseif yy <= -xx*m
        vx = 0.0;
        vy = 0.0;
    else
        % EQUATION 6 OF ZEHNDER AND ALLMENDINGER (2000)
        vx = (sinc/2.0)*(yy/(xx*m)+1.0);
        vy = (sinc/2.0)*(m/2)*((yy/(xx*m))^2.0-1.0);
    end
end
end
```